Journal of Sound and Vibration 329 (2010) 1901–1923

Contents lists available at ScienceDirect

Journal of Sound and Vibration

journal homepage: www.elsevier.com/locate/jsvi

Natural vibration of pre-twisted shear deformable beam systems subject to multiple kinds of initial stresses

A.Y.T. Leung *, J. Fan

Building and Construction, City University of Hong Kong, Hong Kong

ARTICLE INFO

Article history:
Received 15 October 2009
Received in revised form
1 December 2009
Accepted 1 December 2009
Handling Editor: L.G. Tham
Available online 30 December 2009

ABSTRACT

Free vibration and buckling of pre-twisted beams exhibit interesting coupling phenomena between compression, moments and torque and have been the subject of extensive research due to their importance as models of wind turbines and helicopter rotor blades. The paper investigates the influence of multiple kinds of initial stresses due to compression, shears, moments and torque on the natural vibration of pre-twisted straight beam based on the Timoshenko theory. The derivation begins with the three-dimensional Green strain tensor. The nonlinear part of the strain tensor is expressed as a product of displacement gradient to derive the strain energy due to initial stresses. The Frenet formulae in differential geometry are employed to treat the pre-twist. The strain energy due to elasticity and the linear kinetic energy are obtained in classical sense. From the variational principle, the governing equations and the associated natural boundary conditions are derived. It is noted that the first mode increases together with the pre-twisted angle but the second decreases seeming to close the first two modes together for natural frequencies and compressions. The gaps close monotonically as the angle of twist increases for natural frequencies and buckling compressions. However, unlike natural frequencies and compressions, the closeness is not monotonic for buckling shears, moments and torques.

1. Introduction

Free vibration and buckling of pre-twisted beams [1–28] exhibit interesting coupling phenomena between compression, moments and torque and have been the subject of extensive research due to their importance as models of wind turbines and helicopter rotor blades. Rosard [1], Troesch et al. [2] and Diprima and Handelman [3] were about the first few papers that investigated the natural vibration of pre-twisted beams. Subsequent applications to blade and coupling vibration were investigated by Carnegie [4,5], Slyper [6], Anliker and Troesch [7], Dawson [8] and Lin [9]. Gupta and Rao [10], Sisto and Chang [11], Yardimoglu and Yildirim [12] developed the finite elements to study vibration problems of pre-twisted beams or bladings. Celep and Turham [13] included the influence of shear and rotator inertia on the vibration of pre-twisting beams. Rosen et al. [14,15] used principal coordinates and Onipede et al. [16] and Balhaddad and Onipede [17] studied the three dimensional behaviors. Petrov and Geradin [18] presented a nonlinear theory. Banerjee [19,20] introduced an exact solution method of dynamic stiffness. Many works are existed to study vibration problems of pre-twisted beams under axial loadings, including Chen and Keer [21], Lee [22], Liao and Huang [23] and Sakar and

* Corresponding author. Tel.: +852 2788 7600; fax: +852 2788 7612.
E-mail address: Andrew.leung@cityu.edu.hk (A.Y.T. Leung).

0022-460X/$ - see front matter © 2009 Elsevier Ltd. All rights reserved.
doi:10.1016/j.jsv.2009.12.002

Sabuncu [24]. Some recent developments on buckling problems of pre-twisted beams can be found in [25–28]. However, fewer references are contributed to dynamic stability problems of pre-twisted beams subject to shears, moments and torques.

We aim at formulating the influence of multiple kinds of initial stresses due to compression, shears, moments and torque on the natural vibration of pre-twisted straight beam based on the Timoshenko theory. The formulation can be extended to system of many pre-twisted beams from the equilibrium and compatibility consideration. We begin with the three-dimensional Green strain tensor. The nonlinear part of the strain tensor is expressed as a product of displacement gradient to derive the strain energy due to initial stresses. The Frenet formulae in differential geometry are employed to treat the pre-twist. The strain energy due to elasticity and the kinetic energy are obtained in classical sense. From the variational principle, the governing equations and the associated natural boundary conditions are derived.

The p-element method is a kind of method to improve the performance of finite element method by increasing the order of the polynomial shape functions for a fixed mesh. The p-element method has been successfully applied to vibration problems of beams and plates [29–34]. The element displacement is described by linear shape functions plus a variable number of hierarchical functions which are forms of orthogonal Legendre polynomials or trigonometric series. The linear shape functions are used to define the two nodal displacement of the beam and the hierarchical functions are used to provide additional degrees of freedom to the interior of the beam element. The results can be improved by increasing the terms of the additional functions. Only one element is needed to achieve excellent results. Since the Legendre polynomials are proved to be convergent much faster than Fourier series when the beam is of C^0 continuity [34], the Legendre orthogonal polynomials used by Houmat [33] are chosen to solve the vibration and buckling problems of the pre-twisted straight beam in this paper. The vibration problems of Rosen [14] and Banerjee [19,20] are taken as the first example. The natural frequencies obtained by the p-element agree well with Rosen [14] and Banerjee's results [20]. Secondly, to prove the accuracy of the present theory, the results of frequency and buckling shears and compressions of a pre-twisted rectangular cross-section beam are compared with results of ANSYS, and good agreement is found. The influence of the pre-twist angle and rigidity ratio on the first two natural frequencies, buckling loads of the beam with rectangular cross-sections are considered. It is interesting to note that the first natural frequency and compression modes increases together with the angle of twist but the second decreases seeming to close the first two modes together for natural frequencies and compressions. The gaps reduce monotonically as the angle of twist increases for natural frequencies and buckling compressions. However, unlike natural frequencies and compression compressions, the closeness is not monotonic for buckling shears, moments and torques.

2. Incremental strain analysis

In general three-dimensional elasticity analysis, the Green strain tensor is given by

$$e_{ij}=\frac{1}{2}\left(\frac{\partial u_j}{\partial x_i}+\frac{\partial u_i}{\partial x_j}+\frac{\partial u_k}{\partial x_i}\,\frac{\partial u_k}{\partial x_j}\right) \tag{1}$$

which can be written in engineering form in linear and nonlinear parts as

$$\mathbf{e}=\mathbf{e}^0+\mathbf{e}^1 \tag{2}$$

in which

$$\mathbf{e}=\begin{Bmatrix} e_{11}\\ e_{22}\\ e_{33}\\ 2e_{12}\\ 2e_{23}\\ 2e_{31}\end{Bmatrix},\quad \mathbf{e}^0=\begin{Bmatrix} e^0_{11}\\ e^0_{22}\\ e^0_{33}\\ 2e^0_{12}\\ 2e^0_{23}\\ 2e^0_{31}\end{Bmatrix},\quad \mathbf{e}^1=\begin{Bmatrix} e^1_{11}\\ e^1_{22}\\ e^1_{33}\\ 2e^1_{12}\\ 2e^1_{23}\\ 2e^1_{31}\end{Bmatrix},\quad \text{for } e^0_{ij}=\frac{1}{2}\left(\frac{\partial u_j}{\partial x_i}+\frac{\partial u_i}{\partial x_j}\right),\ e^1_{ij}=\frac{1}{2}\frac{\partial u_k}{\partial x_i}\,\frac{\partial u_k}{\partial x_j} \tag{3}$$

However, the nonlinear part $\mathbf{e}^1$ can be rewritten as

$$\mathbf{e}^1=\frac{1}{2}\mathbf{H}\boldsymbol{\varphi}=\frac{1}{2}\begin{bmatrix} \partial\mathbf{u}/\partial x_1 & 0 & 0\\ 0 & \partial\mathbf{u}/\partial x_2 & 0\\ 0 & 0 & \partial\mathbf{u}/\partial x_3\\ \partial\mathbf{u}/\partial x_2 & 0 & \partial\mathbf{u}/\partial x_3\\ \partial\mathbf{u}/\partial x_1 & \partial\mathbf{u}/\partial x_3 & 0\\ 0 & \partial\mathbf{u}/\partial x_2 & \partial\mathbf{u}/\partial x_1\end{bmatrix}\begin{Bmatrix} \partial\mathbf{u}/\partial x_1\\ \partial\mathbf{u}/\partial x_2\\ \partial\mathbf{u}/\partial x_3\end{Bmatrix} \tag{4}$$

where

$$\mathbf{u}(x,y,z)=\begin{Bmatrix}u_1\\u_2\\u_3\end{Bmatrix} \quad \text{and} \quad \boldsymbol{\varphi}=\begin{Bmatrix}\partial\mathbf{u}/\partial x_1\\ \partial\mathbf{u}/\partial x_2\\ \partial\mathbf{u}/\partial x_3\end{Bmatrix}.$$

It is easily proved that

$$(\mathrm{d}\mathbf{H})\boldsymbol{\varphi}=\mathbf{H}(\mathrm{d}\boldsymbol{\varphi})$$

Therefore,

$$\mathrm{d}\mathbf{e}^1=\tfrac{1}{2}(\mathrm{d}\mathbf{H})\boldsymbol{\varphi}+\tfrac{1}{2}\mathbf{H}(\mathrm{d}\boldsymbol{\varphi})=(\mathrm{d}\mathbf{H})\boldsymbol{\varphi}=\mathbf{H}(\mathrm{d}\boldsymbol{\varphi}) \tag{5}$$

Let the stress vector be

$$\boldsymbol{\sigma}=\{\sigma_{11}\ \ \sigma_{22}\ \ \sigma_{33}\ \ \sigma_{12}\ \ \sigma_{23}\ \ \sigma_{31}\}^{\mathrm{T}} \tag{6}$$

then, by direct expansion,

$$\begin{aligned}\mathrm{d}\mathbf{H}^{\mathrm{T}}\boldsymbol{\sigma}&=\mathrm{d}\begin{bmatrix}\frac{\partial\mathbf{u}}{\partial x_1} & 0 & 0 & \frac{\partial\mathbf{u}}{\partial x_2} & 0 & \frac{\partial\mathbf{u}}{\partial x_3}\\ 0 & \frac{\partial\mathbf{u}}{\partial x_2} & 0 & \frac{\partial\mathbf{u}}{\partial x_1} & \frac{\partial\mathbf{u}}{\partial x_3} & 0\\ 0 & 0 & \frac{\partial\mathbf{u}}{\partial x_3} & 0 & \frac{\partial\mathbf{u}}{\partial x_2} & \frac{\partial\mathbf{u}}{\partial x_1}\end{bmatrix}\begin{Bmatrix}\sigma_{11}\\ \sigma_{22}\\ \sigma_{33}\\ \sigma_{12}\\ \sigma_{23}\\ \sigma_{31}\end{Bmatrix}=\begin{Bmatrix}\sigma_{11}\mathrm{d}\left(\frac{\partial\mathbf{u}}{\partial x_1}\right)+\sigma_{12}\mathrm{d}\left(\frac{\partial\mathbf{u}}{\partial x_2}\right)+\sigma_{13}\mathrm{d}\left(\frac{\partial\mathbf{u}}{\partial x_3}\right)\\ \sigma_{21}\mathrm{d}\left(\frac{\partial\mathbf{u}}{\partial x_1}\right)+\sigma_{22}\mathrm{d}\left(\frac{\partial\mathbf{u}}{\partial x_2}\right)+\sigma_{23}\mathrm{d}\left(\frac{\partial\mathbf{u}}{\partial x_3}\right)\\ \sigma_{31}\mathrm{d}\left(\frac{\partial\mathbf{u}}{\partial x_1}\right)+\sigma_{32}\mathrm{d}\left(\frac{\partial\mathbf{u}}{\partial x_2}\right)+\sigma_{33}\mathrm{d}\left(\frac{\partial\mathbf{u}}{\partial x_3}\right)\end{Bmatrix}\\ &=\begin{bmatrix}\sigma_{11}\mathbf{I} & \sigma_{12}\mathbf{I} & \sigma_{13}\mathbf{I}\\ \sigma_{21}\mathbf{I} & \sigma_{22}\mathbf{I} & \sigma_{23}\mathbf{I}\\ \sigma_{31}\mathbf{I} & \sigma_{32}\mathbf{I} & \sigma_{33}\mathbf{I}\end{bmatrix}\mathrm{d}\begin{Bmatrix}\partial\mathbf{u}/\partial x_1\\ \partial\mathbf{u}/\partial x_2\\ \partial\mathbf{u}/\partial x_3\end{Bmatrix}=[\boldsymbol{\sigma}]\mathrm{d}\boldsymbol{\varphi}\end{aligned} \tag{7}$$

When the initial stress vector $\boldsymbol{\sigma}$ in Eq. (6) is sufficiently considered, a second order analysis will be completed. In the following analysis, the non-vanishing strains and stresses are $\{e_{31}\ \ e_{32}\ \ e_{33}\}$ and $\{\sigma_{31}\ \ \sigma_{32}\ \ \sigma_{33}\}$ respectively to satisfy the Timoshenko assumption.

3. Geometry

3.1. The geometry of a general curve with a pre-twisted rate

For a general curve in space whose Cartesian coordinate vector $\mathbf{v}=\mathbf{v}(z)$ is determined by the arc-length coordinate z (in the $\vec{e}_3$ direction to be defined later), then, from differential geometry, the generalized curvatures p, q, and r are defined by

$$\frac{\partial\mathbf{v}}{\partial z}=\mathbf{v}'+\mathbf{K}\mathbf{v},\quad \mathbf{K}=\begin{bmatrix}0 & r & -q\\ -r & 0 & p\\ q & -p & 0\end{bmatrix},\quad \begin{Bmatrix}p\\q\\r\end{Bmatrix}=\begin{Bmatrix}\kappa\sin\chi\\ \kappa\cos\chi\\ \tau+\mu\end{Bmatrix},\quad \mu=\chi' \tag{8}$$

where κ and τ and the curvature and tortuosity of the centerline and χ is the twist of the cross-section to bring the principal axes in alignment with the principal normal and bi-normal, and the prime on χ denotes the derivation with respect to z. If the beam is uniformly twisted when unstressed, then $\chi=\mu z$ and the Frenet formulae is

$$\begin{Bmatrix}p\\q\\r\end{Bmatrix}=\begin{Bmatrix}\kappa\sin\mu z\\ \kappa\cos\mu z\\ \tau+\mu\end{Bmatrix} \tag{9}$$

Consider a twisted straight beam when $\kappa=\tau=0$ but $\mu\neq0$ whose cross-section is shown in Fig. 1. The principal axes are along x ($\vec{e}_1,\vec{N}$) and y ($\vec{e}_2,\vec{B}$) respectively and $\vec{N}$ and $\vec{B}$ are the unit vectors of normal and bi-normal. Along the centerline, the position $\vec{r}(z)$, normal $\vec{N}(z)$, bi-normal $\vec{B}(z)$ and tangent $\vec{T}$ vectors are given respectively by

$$\vec{r}(z)=\begin{Bmatrix}0\\0\\z\end{Bmatrix},\quad \vec{N}(z)=\begin{Bmatrix}\cos\mu z\\ -\sin\mu z\\ 0\end{Bmatrix},\quad \vec{B}(z)=\begin{Bmatrix}\sin\mu z\\ \cos\mu z\\ 0\end{Bmatrix},\quad \vec{T}=\begin{Bmatrix}0\\0\\1\end{Bmatrix} \tag{10}$$

The position vector $\bar{\mathbf{r}}(x,y,z)$ or $\bar{\mathbf{r}}(R,\theta,z)$ of a point on the plane z=constant at polar coordinates (R,θ) away from the centerline is given by

$$\bar{\mathbf{r}}=\mathbf{r}+R(-\cos\theta\mathbf{N}+\sin\theta\mathbf{B})=\begin{Bmatrix}-R\cos\mu z\cos\theta+R\sin\mu z\sin\theta\\ R\sin\mu z\cos\theta+R\cos\mu z\sin\theta\\ z\end{Bmatrix} \tag{11}$$

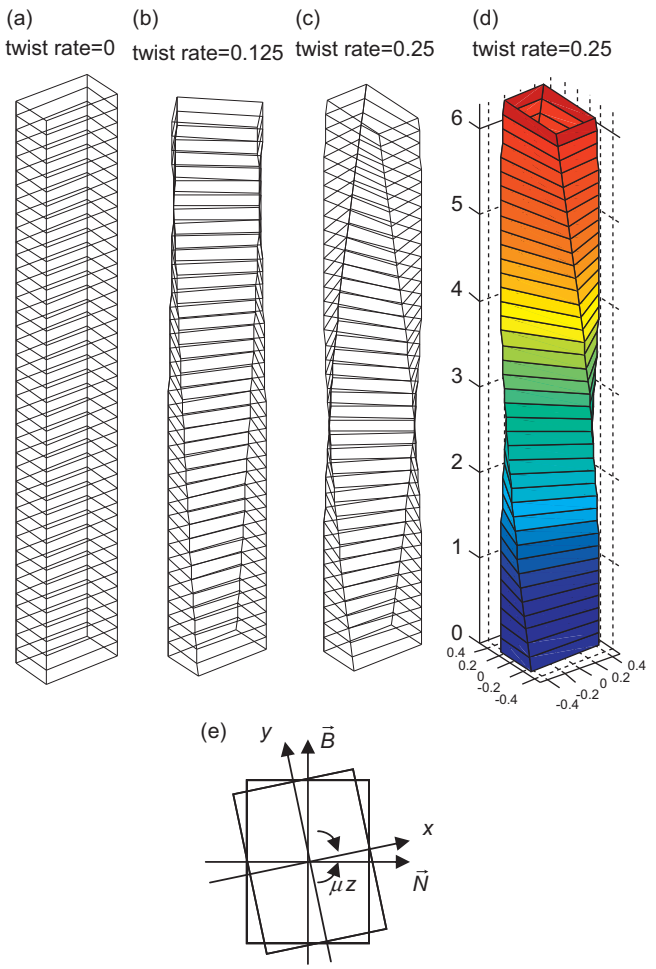

Fig. 1. A pre-twisted straight beam: (a) straight beam, (b) twist rate μ=0.125, (c) twist rate μ=0.25, (d) perspective view of Fig. 1(c), and (e) local coordinate system.

In this paper, the coordinate system (x,y,z) may be interchangeably used with (x_1,x_2,x_3). In all cases, the Jacobian is equal to one.

Consider a straight beam of length l=2π as shown in Fig. 1(a). The rate of pre-twist μ of unit in rad/m is assumed to be constant along the length. Then, the rotation angle measured from the bottom side to the top side of the beam can be defined as the pre-twisted angle $\overline{\mu}=\mu l$. The straight beam with pre-twisted ratio μ=0.125 and 0.25 are shown in Fig. 1(b) and (c), having the corresponding pre-twisted angle $\overline{\mu}=\pi/4$ and $\pi/2$, respectively. Fig. 1(d) gives a perspective view of Fig. 1(c) and (e) depicts the local coordinate system.

When the centerline is straight, $\tau=\kappa=0$, and the Frenet formulae becomes

$$\frac{\mathrm{d}}{\mathrm{d}z}\begin{Bmatrix}\vec{e}_1\\ \vec{e}_2\\ \vec{e}_3\end{Bmatrix}=\begin{bmatrix}0 & \mu & 0\\ -\mu & 0 & 0\\ 0 & 0 & 0\end{bmatrix}\begin{Bmatrix}\vec{e}_1\\ \vec{e}_2\\ \vec{e}_3\end{Bmatrix}\quad\text{or}\quad\vec{\mathbf{e}}'=\mathbf{K}\vec{\mathbf{e}},\ \text{where}\ \mathbf{K}=\begin{bmatrix}0 & \mu & 0\\ -\mu & 0 & 0\\ 0 & 0 & 0\end{bmatrix}\tag{12}$$

3.2. Displacement, strain and external force

The coordinate system attached to the positive face across the centerline along the principle axes for a straight prismatic beam is shown in Fig. 2, assuming the Timoshenko's plane-remain plane cross-section during deformation. Axis 3 is along the centerline, axes 1 and 2 are the principal axes making 1-2-3 a right hand triad.

The displacements and rotations of a rectangular cross-section along the centerline at z are denoted by $\mathbf{r}(z)$ where

$$\mathbf{r}(z)=\begin{bmatrix}\mathbf{v}\\ \boldsymbol{\theta}\end{bmatrix}\tag{13}$$

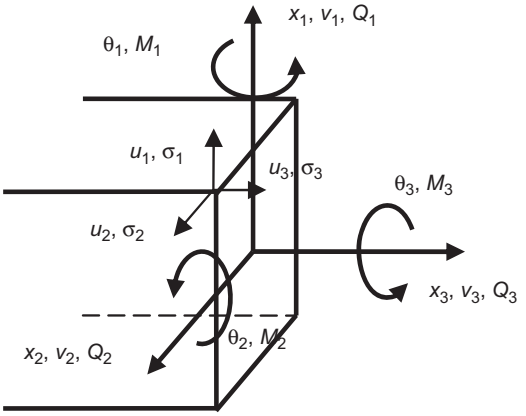

Fig. 2. Displacements and external forces of a straight beam.

where

$$\mathbf{v}=\begin{pmatrix}v_1\\v_2\\v_3\end{pmatrix} \quad \text{and} \quad \boldsymbol{\theta}=\begin{pmatrix}\theta_1\\\theta_2\\\theta_3\end{pmatrix}$$

The Timoshenko assumptions for plane-remain-plane during deformation give

$$\mathbf{u}(x,y,z)=\begin{Bmatrix}u_1\\u_2\\u_3\end{Bmatrix}=\begin{Bmatrix}v_1(z)\\v_2(z)\\v_3(z)\end{Bmatrix}+\begin{bmatrix}0&0&-y\\0&0&x\\y&-x&0\end{bmatrix}\begin{Bmatrix}\theta_1(z)\\\theta_2(z)\\\theta_3(z)\end{Bmatrix}=\begin{bmatrix}1&0&0&0&0&-y\\0&1&0&0&0&x\\0&0&1&y&-x&0\end{bmatrix}\mathbf{r}(z) \tag{14}$$

The Frenet formulae for total differential with respect to z give

$$\mathbf{u}_{,z}=\mathbf{u}'+\mathbf{K}\mathbf{u}=\begin{bmatrix}1&0&0&0&0&-y\\0&1&0&0&0&x\\0&0&1&y&-x&0\end{bmatrix}\mathbf{r}'+\mu\begin{bmatrix}0&1&0&0&0&0\\-1&0&0&0&0&0\\0&0&0&x&y&0\end{bmatrix}\mathbf{r} \tag{15}$$

A prime denotes local differentiation with respect to z. Also,

$$\mathbf{u}_{,x}=\begin{bmatrix}0&0&0&0&0&0\\0&0&0&0&0&1\\0&0&0&0&-1&0\end{bmatrix}\mathbf{r}(z) \quad \text{and} \quad \mathbf{u}_{,y}=\begin{bmatrix}0&0&0&0&0&-1\\0&0&0&0&0&0\\0&0&0&1&0&0\end{bmatrix}\mathbf{r}(z) \tag{16}$$

The non-vanishing strain components e_{3i} are

$$\mathbf{e}=\begin{Bmatrix}e_{31}\\e_{32}\\e_{33}\end{Bmatrix}=\begin{Bmatrix}u_{3,1}\\u_{3,2}\\0\end{Bmatrix}+\frac{\partial}{\partial z}\begin{Bmatrix}u_1\\u_2\\u_3\end{Bmatrix}=\begin{bmatrix}0&\mu&0&0&-1&0&1&0&0&0&0&-y\\-\mu&0&0&1&0&0&0&1&0&0&0&x\\0&0&0&\mu x&\mu y&0&0&0&1&y&-x&0\end{bmatrix}\begin{Bmatrix}\mathbf{r}\\\mathbf{r}'\end{Bmatrix}=\mathbf{b}(x,y)\begin{Bmatrix}\mathbf{r}\\\mathbf{r}'\end{Bmatrix} \tag{17}$$

where a comma subscript represents partial derivative and a prime denotes differential with respect to x_3. For elastic modulus matrix

$$\mathbf{Y}=\begin{bmatrix}G&0&0\\0&G&0\\0&0&E\end{bmatrix}$$

where G, E are the usual elastic modulus, the non-vanishing stresses σ_{3i} are given by

$$\boldsymbol{\sigma}=\begin{Bmatrix}\sigma_{31}\\\sigma_{32}\\\sigma_{33}\end{Bmatrix}=\mathbf{Y}\mathbf{e} \tag{18}$$

which induce the resistance forces Q_i, $i=1,2,3$ on the positive face as shown in Fig. 2 as

$$\begin{Bmatrix}Q_1\\Q_2\\Q_3\end{Bmatrix}=\int\boldsymbol{\sigma}\,\mathrm{d}x\,\mathrm{d}y=\begin{bmatrix}0&\mu GA&0&0&-GA&0&GA&0&0\\-\mu GA&0&0&GA&0&0&0&GA&0\\0&0&0&0&0&0&0&0&EA\end{bmatrix}\begin{Bmatrix}\mathbf{v}\\\boldsymbol{\theta}\\\mathbf{v}'\end{Bmatrix} \tag{19}$$

as well as the resistance moments M_i, $i=1,2,3$

$$\begin{Bmatrix} M_1 \\ M_2 \\ M_3 \end{Bmatrix} = -\int \mathbf{R}\boldsymbol{\sigma}\,\mathrm{d}x\,\mathrm{d}y = \begin{bmatrix} 0 & EI_1\mu & 0 & 0 & 0 & 0 & EI_1 & 0 & 0 \\ -EI_2\mu & 0 & 0 & 0 & 0 & 0 & 0 & EI_2 & 0 \\ 0 & 0 & 0 & 0 & 0 & 0 & 0 & 0 & GJ \end{bmatrix} \begin{Bmatrix} \boldsymbol{\theta} \\ \mathbf{v}' \\ \boldsymbol{\theta}' \end{Bmatrix} \tag{20}$$

where A is the cross-sectional area, $I_1=\int y^2\,\mathrm{d}A=\int x_2^2\,\mathrm{d}A$, $I_2=\int x^2\,\mathrm{d}A=\int x_1^2\,\mathrm{d}A$, and $I_0=I_1+I_2$, and J is the torsion constant. Other area integrals are assumed to be zeros due to double symmetry. Without loss of generality, the effective shear area factor k is taken as one for simplicity, because one can always simply change GA to kGA when needed as will be done in the numerical examples later.

The initial stresses are given by

$$\boldsymbol{\sigma}^0 = \begin{Bmatrix} \sigma_{31}^0 \\ \sigma_{32}^0 \\ \sigma_{33}^0 \end{Bmatrix} = \begin{Bmatrix} Q_1/A \\ Q_2/A \\ Q_3/A \end{Bmatrix} - \begin{bmatrix} 0 & 0 & -y \\ 0 & 0 & x \\ y & -x & 0 \end{bmatrix} \begin{Bmatrix} M_1/I_1 \\ M_2/I_2 \\ M_3/J \end{Bmatrix} \tag{21}$$

Putting the displacement gradient in matrix form, on has

$$\begin{Bmatrix} \mathbf{u}_{,1} \\ \mathbf{u}_{,2} \\ \mathbf{u}_{,3} \end{Bmatrix} = \begin{bmatrix} 0 & 0 & 0 & 0 & 0 & 0 & 0 & 0 & 0 & 0 & 0 & 0 \\ 0 & 0 & 0 & 0 & 0 & 1 & 0 & 0 & 0 & 0 & 0 & 0 \\ 0 & 0 & 0 & 0 & -1 & 0 & 0 & 0 & 0 & 0 & 0 & 0 \\ 0 & 0 & 0 & 0 & 0 & -1 & 0 & 0 & 0 & 0 & 0 & 0 \\ 0 & 0 & 0 & 0 & 0 & 0 & 0 & 0 & 0 & 0 & 0 & 0 \\ 0 & 0 & 0 & 1 & 0 & 0 & 0 & 0 & 0 & 0 & 0 & 0 \\ 0 & \mu & 0 & 0 & 0 & 0 & 1 & 0 & 0 & 0 & 0 & -y \\ -\mu & 0 & 0 & 0 & 0 & 0 & 0 & 1 & 0 & 0 & 0 & x \\ 0 & 0 & 0 & \mu x & \mu y & 0 & 0 & 0 & 1 & y & -x & 0 \end{bmatrix} \begin{Bmatrix} \mathbf{r} \\ \mathbf{r}' \end{Bmatrix} = \mathbf{U}(x,y) \begin{Bmatrix} \mathbf{r} \\ \mathbf{r}' \end{Bmatrix} \tag{22}$$

4. Energy

The steady state kinetic energy with the vibration frequency ω is given by

$$T = \frac{\omega^2}{2}\int \rho \mathbf{r}^{\mathrm{T}}\mathbf{A}_m\mathbf{r}\,\mathrm{d}x_3 \tag{23}$$

where

$$\mathbf{A}_m = \begin{bmatrix} A & 0 & 0 & 0 & 0 & 0 \\ 0 & A & 0 & 0 & 0 & 0 \\ 0 & 0 & A & 0 & 0 & 0 \\ 0 & 0 & 0 & I_1 & 0 & 0 \\ 0 & 0 & 0 & 0 & I_2 & 0 \\ 0 & 0 & 0 & 0 & 0 & I_0 \end{bmatrix} \tag{24}$$

The elastic strain energy density per unit length due to the non-vanishing initial stresses is given by Eq. (7)

$$\begin{aligned} U_\sigma(x_3) &= \frac{1}{2}\int_A \begin{Bmatrix} \mathbf{u}_{,1} \\ \mathbf{u}_{,2} \\ \mathbf{u}_{,3} \end{Bmatrix}^{\mathrm{T}} \begin{bmatrix} 0 & 0 & \sigma_{31}^0\mathbf{I} \\ 0 & 0 & \sigma_{32}^0\mathbf{I} \\ \sigma_{31}^0\mathbf{I} & \sigma_{32}^0\mathbf{I} & \sigma_{33}^0\mathbf{I} \end{bmatrix} \begin{Bmatrix} \mathbf{u}_{,1} \\ \mathbf{u}_{,2} \\ \mathbf{u}_{,3} \end{Bmatrix} \mathrm{d}x\,\mathrm{d}y \\ &= \frac{1}{2}\begin{Bmatrix} \mathbf{r} \\ \mathbf{r}' \end{Bmatrix}^{\mathrm{T}} \int_A \mathbf{U}^{\mathrm{T}} \begin{bmatrix} 0 & 0 & \sigma_{31}^0\mathbf{I} \\ 0 & 0 & \sigma_{32}^0\mathbf{I} \\ \sigma_{31}^0\mathbf{I} & \sigma_{32}^0\mathbf{I} & \sigma_{33}^0\mathbf{I} \end{bmatrix} \mathbf{U}\,\mathrm{d}x\,\mathrm{d}y \begin{Bmatrix} \mathbf{r} \\ \mathbf{r}' \end{Bmatrix} = \frac{1}{2}\begin{Bmatrix} \mathbf{r} \\ \mathbf{r}' \end{Bmatrix}^{\mathrm{T}} \mathbf{A}_\sigma \begin{Bmatrix} \mathbf{r} \\ \mathbf{r}' \end{Bmatrix} \end{aligned} \tag{25}$$

where the initial stress strain energy density matrix $\mathbf{A}_\sigma$ is obtained after integration over the cross-sectional area as

$$\mathbf{A}_\sigma = \begin{bmatrix}
\mu^2 Q_3 & & & & & & & & & & & \\
0 & \mu^2 Q_3 & & & & & & & & & & \\
0 & 0 & 0 & & & & & & & sym & & \\
0 & 0 & 0 & \dfrac{\mu^2 I_2 Q_3}{A} + \dfrac{2 I_2 M_3 \mu}{J} & & & & & & & & \\
0 & 0 & 0 & 0 & \dfrac{\mu^2 I_1 Q_3}{A} + \dfrac{2 I_1 M_3 \mu}{J} & & & & & & & \\
-\mu Q_1 & -\mu Q_2 & 0 & 0 & 0 & 0 & & & & & & \\
0 & \mu Q_3 & 0 & 0 & 0 & -Q_2 & Q_3 & & & & & \\
-\mu Q_3 & 0 & 0 & 0 & 0 & Q_1 & 0 & Q_3 & & & & \\
0 & 0 & 0 & Q_2 - M_2 \mu & M_1 \mu - Q_1 & 0 & 0 & 0 & Q_3 & & & \\
0 & 0 & 0 & 0 & I_1 \left(\dfrac{M_3}{J} + \dfrac{Q_3 \mu}{A} + E\mu \right) & 0 & 0 & 0 & M_1 & Q_3 I_1 / A & & \\
0 & 0 & 0 & -I_2 \left(\dfrac{M_3}{J} + \dfrac{Q_3 \mu}{A} + E\mu \right) & 0 & 0 & 0 & 0 & M_2 & 0 & Q_3 I_2 / A & \\
\mu M_2 & -\mu M_1 & 0 & 0 & 0 & 0 & -M_1 & -M_2 & 0 & 0 & 0 & J Q_3 / A
\end{bmatrix} \tag{26}$$

It is noted that the initial stresses in Eq. (26) relate to strains and displacements, hence, nonlinear displacements have been considered here. The terms involving initial torque M_3 are slightly different from those of some authors and discussions can be found in [35–37]. The total strain energy density per unit length U_0 is the sum of the strain energy density due to initial stresses U_σ represented by $\mathbf{A}_\sigma$ and U_e that due to linear strain by $\mathbf{A}_e$ where

$$U_e = \frac{1}{2} \begin{Bmatrix} \mathbf{r} \\ \mathbf{r}' \end{Bmatrix}^{\mathrm{T}} \int_A \mathbf{b}^{\mathrm{T}} \mathbf{Y} \mathbf{b} \, \mathrm{d}x_1 \, \mathrm{d}x_2 \begin{Bmatrix} \mathbf{r} \\ \mathbf{r}' \end{Bmatrix} = \frac{1}{2} \begin{Bmatrix} \mathbf{r} \\ \mathbf{r}' \end{Bmatrix}^{\mathrm{T}} \mathbf{A}_e \begin{Bmatrix} \mathbf{r} \\ \mathbf{r}' \end{Bmatrix} \tag{27}$$

where $\mathbf{b}$ is from Eq. (17), and

$$\mathbf{A}_e = \begin{bmatrix}
\mu^2 GA & & & & & & & & & & & \\
0 & \mu^2 GA & & & & & & & & & & \\
0 & 0 & 0 & & & & & & & sym & & \\
-\mu GA & 0 & 0 & GA + EI_2 \mu^2 & & & & & & & & \\
0 & -\mu GA & 0 & 0 & GA + EI_1 \mu^2 & & & & & & & \\
0 & 0 & 0 & 0 & 0 & 0 & & & & & & \\
0 & \mu GA & 0 & 0 & -GA & 0 & GA & & & & & \\
-\mu GA & 0 & 0 & GA & 0 & 0 & 0 & GA & & & & \\
0 & 0 & 0 & 0 & 0 & 0 & 0 & 0 & EA & & & \\
0 & 0 & 0 & 0 & I_1 E\mu & 0 & 0 & 0 & 0 & EI_1 & & \\
0 & 0 & 0 & -I_2 E\mu & 0 & 0 & 0 & 0 & 0 & 0 & EI_2 & \\
0 & 0 & 0 & 0 & 0 & 0 & 0 & 0 & 0 & 0 & 0 & GJ
\end{bmatrix} \tag{28}$$

The higher order terms of μ^2 are not negligible and must be retained in numerical simulation. For the convenience of numerical simulation, the non-dimensional equations are given by Eq. (29),

$$\overline{\mu} = \mu l, \quad g = \frac{GAl^2}{EI_1}, \quad r_1 = \frac{I_1}{Al^2}, \quad r_2 = \frac{I_2}{Al^2}, \quad r_0 = \frac{I_0}{Al^2}, \quad r_J = \frac{J}{Al^2},$$

$$\lambda^4 = \frac{\omega^2 \rho A l^4}{EI_1}, \quad q_1 = \frac{Q_1 l^2}{EI_1}, \quad q_2 = \frac{Q_2 l^2}{EI_1}, \quad q_3 = \frac{Q_3 l^2}{EI_1}, \quad m_1 = \frac{M_1 l}{EI_1}, \quad m_2 = \frac{M_2 l}{EI_1}, \quad m_3 = \frac{M_3 l}{EJ} \tag{29}$$

And the non-dimensional matrices of $\mathbf{A}_e$, $\mathbf{A}_m$ and $\mathbf{A}_\sigma$ are given in the following Eqs. (30)–(32), respectively:

$$a_e = \frac{EI_1}{l^2}\begin{bmatrix}
\overline{\mu}^2 g & & & & & & & & & & & \\
0 & \overline{\mu}^2 g & & & & & & & & & & \\
0 & 0 & 0 & & & & & & sym & & & \\
-\overline{\mu} g & 0 & 0 & g+\overline{\mu}^2 r_2/r_1 & & & & & & & & \\
0 & -\overline{\mu} g & 0 & 0 & g+\overline{\mu}^2 & & & & & & & \\
0 & 0 & 0 & 0 & 0 & 0 & & & & & & \\
0 & \overline{\mu} g & 0 & 0 & -g & 0 & g & & & & & \\
-\overline{\mu} g & 0 & 0 & g & 0 & 0 & 0 & g & & & & \\
0 & 0 & 0 & 0 & 0 & 0 & 0 & 0 & 1/r_1 & & & \\
0 & 0 & 0 & 0 & \overline{\mu} & 0 & 0 & 0 & 0 & 1 & & \\
0 & 0 & 0 & -\overline{\mu} r_2/r_1 & 0 & 0 & 0 & 0 & 0 & 0 & r_2/r_1 & \\
0 & 0 & 0 & 0 & 0 & 0 & 0 & 0 & 0 & 0 & 0 & g r_J
\end{bmatrix} \tag{30}$$

$$a_m = \frac{EI_1}{l^2}\begin{bmatrix}
1 & & & & & & \\
 & 1 & & & & & \\
 & & 1 & & & & \\
 & & & r_1 & & & \\
 & & & & r_2 & & \\
 & & & & & r_0
\end{bmatrix} \tag{31}$$

$$a_\sigma = \frac{EI_1}{l^2}\begin{bmatrix}
\overline{\mu}^2 q_3 & & & & & & & & & & & \\
0 & \overline{\mu}^2 q_3 & & & & & & & & & & \\
0 & 0 & 0 & & & & & & sym & & & \\
0 & 0 & 0 & 2\overline{\mu} m_3 r_2/r_1+\overline{\mu}^2 q_3 r_2 & & & & & & & & \\
0 & 0 & 0 & 0 & 2\overline{\mu} m_3+\overline{\mu}^2 q_3 r_1 & & & & & & & \\
-\overline{\mu} q_1 & -\overline{\mu} q_2 & 0 & 0 & 0 & 0 & & & & & & \\
0 & \overline{\mu} q_3 & 0 & 0 & 0 & -q_2 & q_3 & & & & & \\
-\overline{\mu} q_3 & 0 & 0 & 0 & 0 & q_1 & 0 & q_3 & & & & \\
0 & 0 & 0 & q_2-\overline{\mu} m_2 & \overline{\mu} m_1-q_1 & 0 & 0 & 0 & q_3 & & & \\
0 & 0 & 0 & 0 & m_3+\overline{\mu} q_3 r_1 & 0 & 0 & 0 & m_1 & q_3 r_1 & & \\
0 & 0 & 0 & -m_3-\overline{\mu} q_3 r_2 & 0 & 0 & 0 & 0 & m_2 & 0 & q_3 r_2 & \\
\overline{\mu} m_2 & -\overline{\mu} m_1 & 0 & 0 & 0 & 0 & -m_1 & -m_2 & 0 & 0 & 0 & q_3 r_J
\end{bmatrix} \tag{32}$$

5. p-elements for pre-twisted straight beams

5.1. Shape functions

The generalized nodal displacements of the pre-twisted straight beam can be obtained from Eq. (13),

$$\mathbf{q}_g = [v_1^b \;\; v_2^b \;\; v_3^b \;\; \theta_1^b \;\; \theta_2^b \;\; \theta_3^b \;\; v_1^t \;\; v_2^t \;\; v_3^t \;\; \theta_1^t \;\; \theta_2^t \;\; \theta_3^t]^{\mathrm{T}} \tag{33}$$

where the superscript '*b*' and '*t*' means the displacements on the bottom (negative) end and the top (positive) end of the beam according to finite element convention. The displacement $\mathbf{u}$ of a beam subject to constant external forces Q_1, Q_2, Q_3, M_1, M_2 and M_3 is given by

$$\mathbf{u} = \mathbf{N}\mathbf{q} \tag{34}$$

where $\mathbf{N}$ is the shape functions for the pre-twisted straight beam, $\mathbf{q} = \begin{bmatrix}\mathbf{q}_g \\ \mathbf{q}_i\end{bmatrix}$, $\mathbf{q}_g$ is the generalized nodal displacements defined in Eq. (33) and $\mathbf{q}_i$ is the internal freedoms of the beams.

$$\mathbf{q}_i = [t_{v_1} \;\; t_{v_2} \;\; t_{v_3} \;\; t_{\theta_1} \;\; t_{\theta_2} \;\; t_{\theta_3}]^{\mathrm{T}} \tag{35}$$

The shape functions satisfying the displacement continuity at element interface for a pre-twisted straight beam are as following:

$$\mathbf{N}(\xi)=\begin{bmatrix}\mathbf{N}_{v_1}\\ \mathbf{N}_{v_2}\\ \mathbf{N}_{v_3}\\ \mathbf{N}_{\theta_1}\\ \mathbf{N}_{\theta_2}\\ \mathbf{N}_{\theta_3}\end{bmatrix}=\begin{bmatrix}\overline{f}_i(\xi) & 0 & 0 & 0 & 0 & 0\\ 0 & \overline{f}_i(\xi) & 0 & 0 & 0 & 0\\ 0 & 0 & \overline{f}_i(\xi) & 0 & 0 & 0\\ 0 & 0 & 0 & \overline{f}_i(\xi) & 0 & 0\\ 0 & 0 & 0 & 0 & \overline{f}_i(\xi) & 0\\ 0 & 0 & 0 & 0 & 0 & \overline{f}_i(\xi)\end{bmatrix} \tag{36}$$

where $\overline{f}_i(\xi)$ is the C^0 polynomial series which has used by Houmat [33] giving in Appendix A, and the overbar on $f_i(\xi)$ denotes that ξ is mapped from $(-1,1)$ to $(0,1)$, then $\xi=x_3/l$ $(0<\xi<1)$ is the non-dimensional length, and l is the length of beam, and $i=1,2,\ldots,p+2$, p is the number of internal degrees of freedom.

5.2. Stiffness matrix, mass matrix and geometric matrices

The equation of the eigenvalue problem of the pre-twisted straight beams is

$$(\mathbf{K}-\omega^2\mathbf{M}-Q_1\mathbf{G}_{Q_1}-Q_2\mathbf{G}_{Q_2}-Q_3\mathbf{G}_{Q_3}-M_1\mathbf{G}_{M_1}-M_2\mathbf{G}_{M_2}-M_3\mathbf{G}_{M_3})\mathbf{q}=0 \tag{37}$$

where Q_1, Q_2, Q_3, M_1, M_2, M_3 are the external forces. Then the stiffness matrix, mass matrix and geometric stiffness matrix can be obtained as follows:

$$\mathbf{K}=\sum_e\mathbf{K}^e,\quad \mathbf{M}=\sum_e\mathbf{M}^e,\quad \mathbf{G}=\sum_e\mathbf{G}^e \tag{38}$$

where

$$\mathbf{K}^e=\frac{1}{2}\int_0^l\begin{pmatrix}\mathbf{N}\\ \mathrm{d}(\mathbf{N})/\mathrm{d}x_3\end{pmatrix}^{\mathrm{T}}\mathbf{A}_e\begin{pmatrix}\mathbf{N}\\ \mathrm{d}(\mathbf{N})/\mathrm{d}x_3\end{pmatrix}\mathrm{d}x_3 \tag{39a}$$

$$\mathbf{M}^e=\frac{\rho}{2}\int_0^l\mathbf{N}^{\mathrm{T}}\mathbf{A}_m\mathbf{N}\,\mathrm{d}x_3 \tag{39b}$$

Table 1
Convergence of natural frequencies with comparison to existing results (rad/s).

Number of polynomial terms	Mode number				
	1	2	3	4	5
Present (p=12) (k=1)	3.4718	13.341	25.1658	56.3647	103.2249
Present (p=4) (k=1/1.2)	3.4722	13.3646	25.3361	61.5881	104.7998
Present (p=6) (k=1/1.2)	3.4718	13.3409	25.1663	56.4761	103.511
Present (p=8) (k=1/1.2)	3.4718	13.3409	25.1656	56.3649	103.2283
Present (p=10) (k=1/1.2)	3.4718	13.3409	25.1656	56.3642	103.2194
Present (p=12) (k=1/1.2)	3.4718	13.3409	25.1656	56.3642	103.2193
Banerjee [20] Timoshenko theory	3.4715	13.340	25.165	56.363	103.20
Banerjee [19] Bernoulli–Euler theory	3.4717	13.347	25.171	56.372	103.263
Rosen [14]	3.4726	13.2740	25.2700	56.3009	103.200

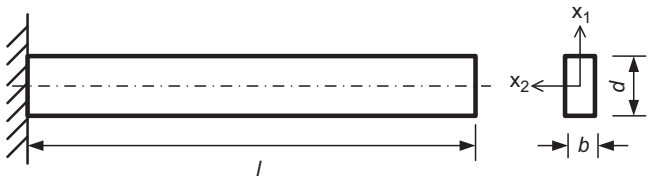

Fig. 3. The dimensions of the cantilevered beam.

$$\mathbf{G}^e = \frac{1}{2}\int_0^l F_{QM}\begin{pmatrix}\mathbf{N}\\ \mathrm{d}(\mathbf{N})/\mathrm{d}x_3\end{pmatrix}^{\mathrm{T}}\mathbf{A}_\sigma\begin{pmatrix}\mathbf{N}\\ \mathrm{d}(\mathbf{N})/\mathrm{d}x_3\end{pmatrix}\mathrm{d}x_3 \tag{39c}$$

where F_{QM} represents the internal forces due to external forces Q_1, Q_2, Q_3, M_1, M_2 or M_3.

By non-dimension, the equation of the eigenvalue problem of the pre-twisted straight beams given in Eq. (38) becomes

$$(\overline{\mathbf{K}}-\lambda^4\overline{\mathbf{M}}-q_1\overline{\mathbf{G}}_{q_1}-q_2\overline{\mathbf{G}}_{q_2}-q_3\overline{\mathbf{G}}_{q_3}-m_1\overline{\mathbf{G}}_{m_1}-m_2\overline{\mathbf{G}}_{m_2}-m_3\overline{\mathbf{G}}_{m_3})\overline{\mathbf{q}}=0 \tag{40}$$

where

$$\overline{\mathbf{K}}^e = \frac{1}{2}\int_0^1\begin{pmatrix}\mathbf{N}(\xi)\\ \mathrm{d}[\mathbf{N}(\xi)]/\mathrm{d}\xi\end{pmatrix}^{\mathrm{T}}\mathbf{a}_e\begin{pmatrix}\mathbf{N}(\xi)\\ \mathrm{d}[\mathbf{N}(\xi)]/\mathrm{d}\xi\end{pmatrix}\mathrm{d}\xi \tag{41a}$$

$$\overline{\mathbf{M}}^e = \frac{1}{2}\int_0^1 \mathbf{N}^{\mathrm{T}}(\xi)\mathbf{a}_m\mathbf{N}(\xi)\,\mathrm{d}\xi \tag{41b}$$

$$\overline{\mathbf{G}}^e = \frac{1}{2}\int_0^1 \overline{F}_{QM}\begin{pmatrix}\mathbf{N}(\xi)\\ \mathrm{d}[\mathbf{N}(\xi)]/\mathrm{d}\xi\end{pmatrix}^{\mathrm{T}}\mathbf{a}_\sigma\begin{pmatrix}\mathbf{N}(\xi)\\ \mathrm{d}[\mathbf{N}(\xi)]/\mathrm{d}\xi\end{pmatrix}\mathrm{d}\xi \tag{41c}$$

Table 2
Frequency λ and buckling loads load parameters $\sqrt{q_1}$, $\sqrt{q_2}$, $\sqrt{q_3}$ of a pre-twisted clamped-free beam with l=1 m, b=1/1.5 mm, d=1.5 mm, $\overline{\mu}=\pi/2$ and compared with results of ANSYS.

Frequency and buckling loads	Mode number					
	1	2	3	4	5	6
λ	1.8961	2.6642	5.0230	6.3181	8.7722	10.0726
ANSYS	1.8964	2.6627	5.0534	6.2238	8.9357	9.9428
$\sqrt{q_1}$	2.4189	4.0885	5.2092	6.1253	6.9350	7.7277
ANSYS	2.4285	4.1393	5.2589	6.1830	6.9881	7.7117
$\sqrt{q_2}$	2.2489	3.5725	4.5218	5.3056	6.0416	6.7899
ANSYS	2.2389	3.5750	4.5244	5.3069	5.9910	6.6083
$\sqrt{q_3}$	1.6290	2.8622	5.9021	7.1493	10.5829	11.5056
ANSYS	1.6383	2.8025	6.0927	7.0194	10.4904	11.7231

Table 3
The relative error when taking ($J\neq I_0$) and ($J=I_0$) for frequency λ and buckling loads parameters $\sqrt{q_1}$, $\sqrt{q_2}$, $\sqrt{q_3}$, $\sqrt{m_1}$, $\sqrt{m_2}$ and m_3 of a pre-twisted clamped-free beam with l=1 m, b=1/1.5 mm, d=1.5 mm, $\overline{\mu}=\pi/2$.

Frequency and buckling loads	Mode number					
	1	2	3	4	5	6
λ	0.0004	0	0	0.0001	0	0
$\sqrt{q_1}$	20.4370	20.4370	20.4369	20.4369	20.4368	20.4367
$\sqrt{q_2}$	20.4370	20.4370	20.4370	20.4370	20.4370	20.4369
$\sqrt{q_3}$	0	0	0	0	0	0
$\sqrt{m_1}$	20.4370	20.4370	20.4370	20.4370	20.4369	20.4369
$\sqrt{m_2}$	20.4370	20.4370	20.4370	20.4370	20.4369	20.4369
m_3 (−)	0	0	0	0	0	0
m_3 (+)	0	0	0	0	0	0

Table 4
The flexural rigidity ratio r when the width d varying from 1 to 1.4 (i=1–5).

d (mm)	1	1.1	1.2	1.3	1.4
d/b	1	1.21	1.44	1.69	1.96
I_0 (mm^4)	0.1667	0.1697	0.1779	0.1901	0.2059
J (mm^4)	0.1406	0.1382	0.1323	0.1244	0.1156
$r_i=I_2/I_1$	1	1.4641	2.0736	2.8561	3.8416

Table 5
(a) Influence of pre-twist angle $\overline{\mu}$ and rigidity ratio r on natural frequency λ. (b) Influence of pre-twist angle $\overline{\mu}$ and rigidity ratio r on buckling loads $\sqrt{q_3}$. (c) Influence of pre-twist angle $\overline{\mu}$ and rigidity ratio r on buckling loads $\sqrt{q_1}$. (d) Influence of pre-twist angle $\overline{\mu}$ and rigidity ratio r on buckling loads $\sqrt{q_2}$. (e) Influence of pre-twist angle $\overline{\mu}$ and rigidity ratio r on buckling loads $\sqrt{m_1}$. (f) Influence of pre-twist angle $\overline{\mu}$ and rigidity ratio r on buckling loads $\sqrt{m_2}$. (g) Influence of pre-twist angle $\overline{\mu}$ and rigidity ratio r on buckling loads m_3 ($-$). (h) Influence of pre-twist angle $\overline{\mu}$ and rigidity ratio r on buckling loads m_3 ($+$).

$\overline{\mu}$	Mode 1					Mode 2				
	r_1	r_2	r_3	r_4	r_5	r_1	r_2	r_3	r_4	r_5
(a)										
0	1.8751	1.8751	1.8751	1.8751	1.8751	1.8751	2.0626	2.2501	2.4376	2.6251
$\pi/4$	1.8751	1.8773	1.8786	1.8795	1.8801	1.8751	2.0591	2.2412	2.4207	2.5968
$\pi/2$	1.8751	1.8834	1.8886	1.8921	1.8945	1.8751	2.0495	2.2172	2.3767	2.5262
$3\pi/4$	1.8751	1.8923	1.9035	1.9110	1.9161	1.8751	2.0360	2.1852	2.3207	2.4416
π	1.8751	1.9025	1.9207	1.9332	1.9418	1.8751	2.0217	2.1525	2.2665	2.3638
$5\pi/4$	1.8751	1.9122	1.9375	1.9550	1.9673	1.8751	2.0090	2.1246	2.2221	2.3028
$3\pi/2$	1.8751	1.9200	1.9512	1.9731	1.9887	1.8751	1.9993	2.1040	2.1903	2.2603
$7\pi/4$	1.8751	1.9255	1.9612	1.9865	2.0046	1.8751	1.9927	2.0902	2.1695	2.2329
2π	1.8751	1.9294	1.9682	1.9960	2.0160	1.8751	1.9882	2.0810	2.1557	2.2149
(b)										
0	1.5708	1.5708	1.5708	1.5708	1.5708	1.5708	1.9007	2.2619	2.6546	3.0788
$\pi/4$	1.5708	1.5769	1.5807	1.5830	1.5846	1.5708	1.8889	2.2275	2.5791	2.9310
$\pi/2$	1.5708	1.5943	1.6088	1.6183	1.6246	1.5708	1.8581	2.1438	2.4144	2.6569
$3\pi/4$	1.5708	1.6192	1.6507	1.6717	1.6860	1.5708	1.8190	2.0474	2.2467	2.4125
π	1.5708	1.6461	1.6976	1.7331	1.7579	1.5708	1.7826	1.9656	2.1166	2.2370
$5\pi/4$	1.5708	1.6674	1.7364	1.7856	1.8208	1.5708	1.7573	1.9126	2.0370	2.1343
$3\pi/2$	1.5708	1.678	1.7566	1.8139	1.8555	1.5708	1.7462	1.8905	2.0055	2.0951
$7\pi/4$	1.5708	1.6817	1.7641	1.8247	1.8693	1.5708	1.7429	1.8845	1.9976	2.0861
2π	1.5708	1.6850	1.7707	1.8342	1.8812	1.5708	1.7397	1.8784	1.9891	2.0758
(c)										
0	1.7177	1.794	1.8534	1.8995	1.9355	2.7448	2.8667	2.9617	3.0354	3.0928
$\pi/4$	1.7177	1.8246	1.9064	1.9688	2.0167	2.7448	2.9288	3.0709	3.1800	3.2639
$\pi/2$	1.7177	1.8926	2.0357	2.1501	2.2403	2.7448	3.0494	3.3165	3.5469	3.7426
$3\pi/4$	1.7177	1.9345	2.1279	2.2960	2.4391	2.7448	3.0626	3.3393	3.5769	3.7799
π	1.7177	1.9116	2.0760	2.2114	2.3208	2.7448	2.9868	3.1860	3.3503	3.4859
$5\pi/4$	1.7177	1.8700	1.9894	2.0815	2.1523	2.7448	2.9685	3.1593	3.3181	3.4478
$3\pi/2$	1.7177	1.8559	1.9634	2.0462	2.1098	2.7448	3.0229	3.2530	3.4385	3.5859
$7\pi/4$	1.7177	1.8666	1.9842	2.0755	2.1462	2.7448	3.0745	3.3624	3.6059	3.8063
2π	1.7177	1.8783	2.0071	2.1086	2.1877	2.7448	3.0230	3.2529	3.4380	3.5847
(d)										
0	1.7177	1.9734	2.2241	2.4694	2.7096	2.7448	3.1534	3.5540	3.9460	4.3299
$\pi/4$	1.7177	1.9285	2.1146	2.2747	2.4101	2.7448	3.0666	3.3479	3.5889	3.7928
$\pi/2$	1.7177	1.8533	1.9584	2.0390	2.1009	2.7448	2.9482	3.1101	3.2370	3.3360
$3\pi/4$	1.7177	1.8198	1.8978	1.9574	2.0031	2.7448	2.9316	3.0755	3.1856	3.2700
π	1.7177	1.8371	1.9286	1.9984	2.0519	2.7448	3.0035	3.2136	3.3794	3.5087
$5\pi/4$	1.7177	1.8737	1.9968	2.0922	2.1657	2.7448	3.0404	3.3085	3.5471	3.7547
$3\pi/2$	1.7177	1.8899	2.0304	2.1423	2.2304	2.7448	2.9663	3.1416	3.2788	3.3857
$7\pi/4$	1.7177	1.8786	2.0078	2.1093	2.1885	2.7448	2.9222	3.0594	3.1654	3.2475
2π	1.7177	1.8671	1.985	2.0768	2.1478	2.7448	2.9659	3.1405	3.2768	3.3829
(e)										
0	1.0747	1.2347	1.3916	1.545	1.6953	1.8615	2.1386	2.4103	2.6761	2.9364
$\pi/4$	1.0747	1.1965	1.3005	1.3872	1.4583	1.8615	2.0947	2.3051	2.4915	2.6543
$\pi/2$	1.0747	1.1456	1.1997	1.2409	1.2725	1.8615	2.0319	2.1708	2.2810	2.3672
$3\pi/4$	1.0747	1.1412	1.1921	1.2310	1.2608	1.8615	2.0152	2.1342	2.2252	2.2947
π	1.0747	1.1715	1.2483	1.3081	1.3544	1.8615	2.0339	2.1793	2.2994	2.3968
$5\pi/4$	1.0747	1.1874	1.2806	1.3555	1.4151	1.8615	2.0194	2.1536	2.2673	2.3632
$3\pi/2$	1.0747	1.1718	1.2492	1.3100	1.3573	1.8615	1.9842	2.0780	2.1494	2.2040
$7\pi/4$	1.0747	1.1615	1.2293	1.2817	1.3220	1.8615	1.9906	2.0905	2.1671	2.2259
2π	1.0747	1.1718	1.2495	1.3105	1.3582	1.8615	2.0270	2.1546	2.2514	2.3248
(f)										
0	1.0747	1.1225	1.1596	1.1885	1.2110	1.8615	1.9441	2.0086	2.0585	2.0974
$\pi/4$	1.0747	1.1495	1.2071	1.2512	1.2851	1.8615	1.9754	2.0635	2.1314	2.1838
$\pi/2$	1.0747	1.2009	1.3094	1.4001	1.4744	1.8615	2.0330	2.1783	2.3020	2.4074
$3\pi/4$	1.0747	1.2071	1.3242	1.4253	1.5109	1.8615	2.0422	2.1875	2.3022	2.3923
π	1.0747	1.1715	1.2483	1.3081	1.3544	1.8615	2.0339	2.1793	2.2994	2.3968
$5\pi/4$	1.0747	1.1567	1.2201	1.2686	1.3058	1.8615	2.0499	2.2114	2.3460	2.4559
$3\pi/2$	1.0747	1.1718	1.2492	1.3100	1.3573	1.8615	2.0800	2.2679	2.4251	2.5537
$7\pi/4$	1.0747	1.1825	1.2706	1.3413	1.3971	1.8615	2.0740	2.2576	2.4130	2.5426
2π	1.0747	1.1718	1.2495	1.3105	1.3582	1.8615	2.0270	2.1546	2.2514	2.3248
(g)										
0	1.5708	1.3599	1.1570	0.9836	0.8421	1.5708	1.7255	1.7867	1.7701	1.7015
$\pi/4$	1.5708	1.4483	1.2916	1.1294	0.9798	1.5708	1.6250	1.6136	1.5591	1.4797

Table 5 (*continued*)

$\bar{\mu}$	Mode 1					Mode 2				
	r_1	r_2	r_3	r_4	r_5	r_1	r_2	r_3	r_4	r_5
$\pi/2$	1.5708	1.5412	1.4619	1.3491	1.2197	1.5708	1.5439	1.4789	1.3942	1.3016
$3\pi/4$	1.5708	1.4946	1.3944	1.2867	1.1807	1.5708	1.5985	1.5744	1.5110	1.4216
π	1.5708	1.4826	1.3679	1.2462	1.1287	1.5708	1.6062	1.5884	1.5329	1.4544
$5\pi/4$	1.5708	1.5037	1.3985	1.2761	1.1522	1.5708	1.5802	1.5411	1.4723	1.3877
$3\pi/2$	1.5708	1.5417	1.4651	1.3592	1.2404	1.5708	1.5436	1.4776	1.3912	1.2968
$7\pi/4$	1.5708	1.5154	1.4277	1.3259	1.2216	1.5708	1.5725	1.5240	1.4409	1.3381
2π	1.5708	1.5063	1.4086	1.2971	1.1844	1.5708	1.5805	1.5405	1.4675	1.3757
(h)										
0	1.5708	1.3599	1.1570	0.9836	0.8421	1.5708	1.7255	1.7867	1.7701	1.7015
$\pi/4$	1.5708	1.3077	1.0957	0.9307	0.8014	1.5708	1.8254	1.9824	2.0162	1.9523
$\pi/2$	1.5708	1.3007	1.1019	0.9510	0.8326	1.5708	1.8927	2.1715	2.2875	2.2119
$3\pi/4$	1.5708	1.3339	1.1613	1.0277	0.9199	1.5708	1.8837	2.2593	2.5719	2.4029
π	1.5708	1.3961	1.2587	1.1457	1.0496	1.5708	1.7807	2.0018	2.1257	1.9305
$5\pi/4$	1.5708	1.4728	1.3766	1.2867	1.2031	1.5708	1.6423	1.6429	1.5483	1.3927
$3\pi/2$	1.5708	1.5385	1.4462	1.3177	1.1815	1.5708	1.5462	1.4920	1.4247	1.3516
$7\pi/4$	1.5708	1.4890	1.3736	1.2483	1.1274	1.5708	1.5963	1.5739	1.5211	1.4486
2π	1.5708	1.4847	1.3766	1.2639	1.1558	1.5708	1.6073	1.5895	1.5291	1.4383

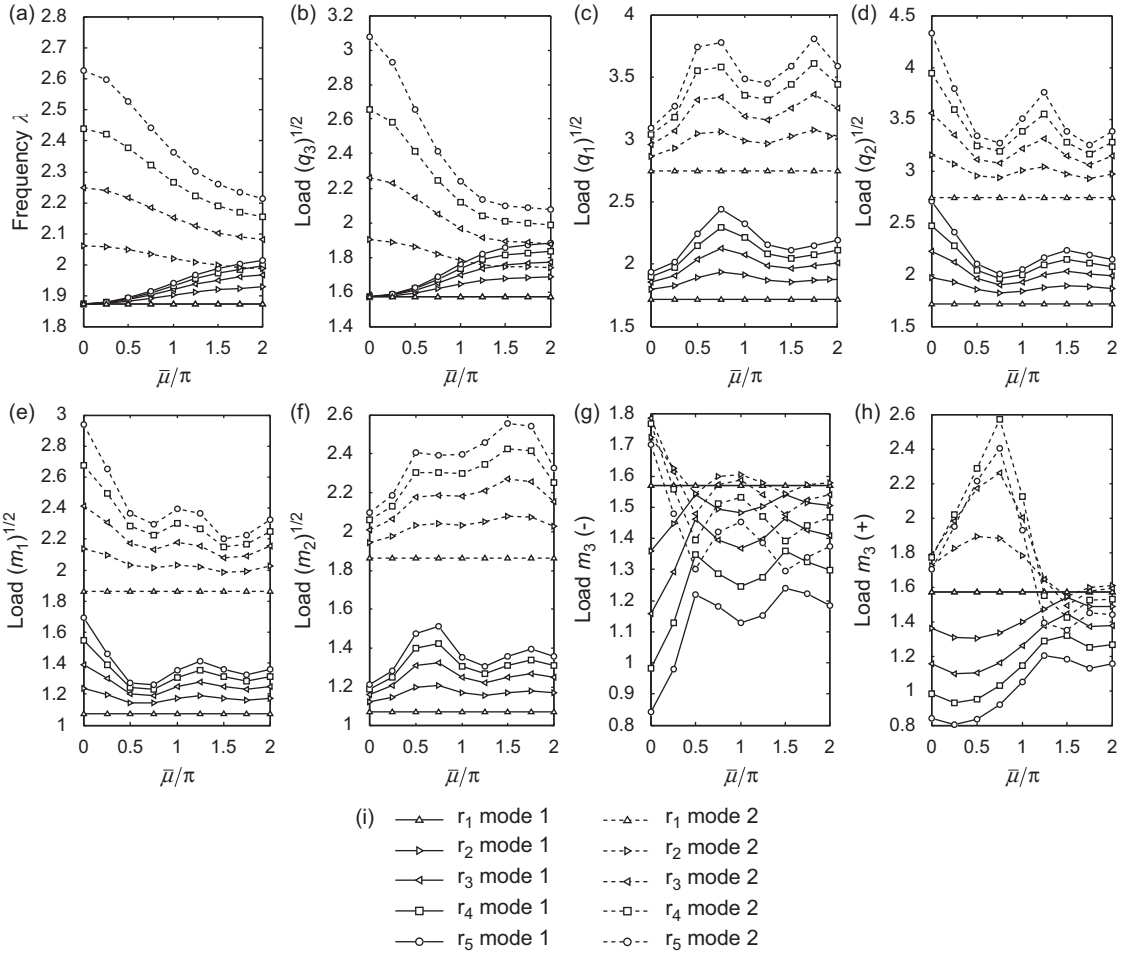

Fig. 4. Natural frequencies and buckling loads under the influence of initial twist angle and flexural rigidity ratio: (a) natural frequency λ, (b) buckling loads $\sqrt{q_3}$, (c) buckling loads $\sqrt{q_1}$, (d) buckling loads $\sqrt{q_2}$, (e) buckling loads $\sqrt{m_1}$, (f) buckling loads $\sqrt{m_2}$, (g) buckling loads m_3 (−), (h) buckling loads m_3 (+), and (i) legend for Figs. 4(a–h).

where the overbar denotes the non-dimensional matrices of $\mathbf{K}^e$, $\mathbf{M}^e$, $\mathbf{G}^e_{q_1}$, $\mathbf{G}^e_{q_2}$, $\mathbf{G}^e_{q_3}$, $\mathbf{G}^e_{m_1}$, $\mathbf{G}^e_{m_2}$ and $\mathbf{G}^e_{m_3}$, non-dimensional displacement vector $\mathbf{q}$, and non-dimensional internal forces F_{QM}.

For a pre-twisted straight beam clamped on one end and free on the other end and is subject only to axial loads Q_3 and/or torque M_3 on the free end, the internal forces will be constant along the length of the beam. However, when the beam is subject to end shears Q_1 or Q_2 or end moments M_1 or M_2, since the beam is pre-twisted, the axes 1 and 2 of the current plane has a twisted angle $\mu\tilde{z}$ with the free-end, therefore, the internal forces become functions of $\mu\tilde{z}$. The internal forces due to end forces Q_1, Q_2, M_1 or M_2 along the length of the beam are given in Eqs. (42a–d), respectively.

$$\tilde{Q}_1\neq 0,\quad \tilde{Q}_2=0,\quad \tilde{M}_1=0,\quad \tilde{M}_2=0 \qquad\qquad \tilde{Q}_1=0,\quad \tilde{Q}_2\neq 0,\quad \tilde{M}_1=0,\quad \tilde{M}_2=0$$

$$\begin{cases} Q_1=\tilde{Q}_1\cos(\mu\tilde{z}) \\ Q_2=-\tilde{Q}_1\sin(\mu\tilde{z}) \\ M_1=\tilde{Q}_1\tilde{z}\sin(\mu\tilde{z}) \\ M_2=\tilde{Q}_1\tilde{z}\cos(\mu\tilde{z}) \end{cases} \qquad \begin{cases} Q_1=\tilde{Q}_2\sin(\mu\tilde{z}) \\ Q_2=\tilde{Q}_2\cos(\mu\tilde{z}) \\ M_1=-\tilde{Q}_2\tilde{z}\cos(\mu\tilde{z}) \\ M_2=\tilde{Q}_2\tilde{z}\sin(\mu\tilde{z}) \end{cases} \tag{42a,b}$$

$$\tilde{Q}_1=0,\quad \tilde{Q}_2=0,\quad \tilde{M}_1\neq 0,\quad \tilde{M}_2=0 \qquad\qquad \tilde{Q}_1=0,\quad \tilde{Q}_2=0,\quad \tilde{M}_1=0,\quad \tilde{M}_2\neq 0$$

$$\begin{cases} Q_1=0 \\ Q_2=0 \\ M_1=\tilde{M}_1\cos(\mu\tilde{z}) \\ M_2=-\tilde{M}_1\sin(\mu\tilde{z}) \end{cases} \qquad \begin{cases} Q_1=0 \\ Q_2=0 \\ M_1=\tilde{M}_2\sin(\mu\tilde{z}) \\ M_2=\tilde{M}_2\cos(\mu\tilde{z}) \end{cases} \tag{42c,d}$$

where the curly overbar '$\sim$'on Q_1, Q_2, M_1 or M_2 denotes the external forces applied on the free end of the cantilevered straight beam and $\tilde{z}=l-x_3=l(1-\xi)$ then $\mu\tilde{z}=\overline{\mu}(1-\xi)$.

The coefficients of the stiffness matrix $\overline{\mathbf{K}}^e$, mass matrix $\overline{\mathbf{M}}^e$ and geometric stiffness matrices $\overline{\mathbf{G}}^e_{q_1}$, $\overline{\mathbf{G}}^e_{q_2}$, $\overline{\mathbf{G}}^e_{q_3}$, $\overline{\mathbf{G}}^e_{m_1}$, $\overline{\mathbf{G}}^e_{m_2}$ and $\overline{\mathbf{G}}^e_{m_3}$ are given in Appendix B.

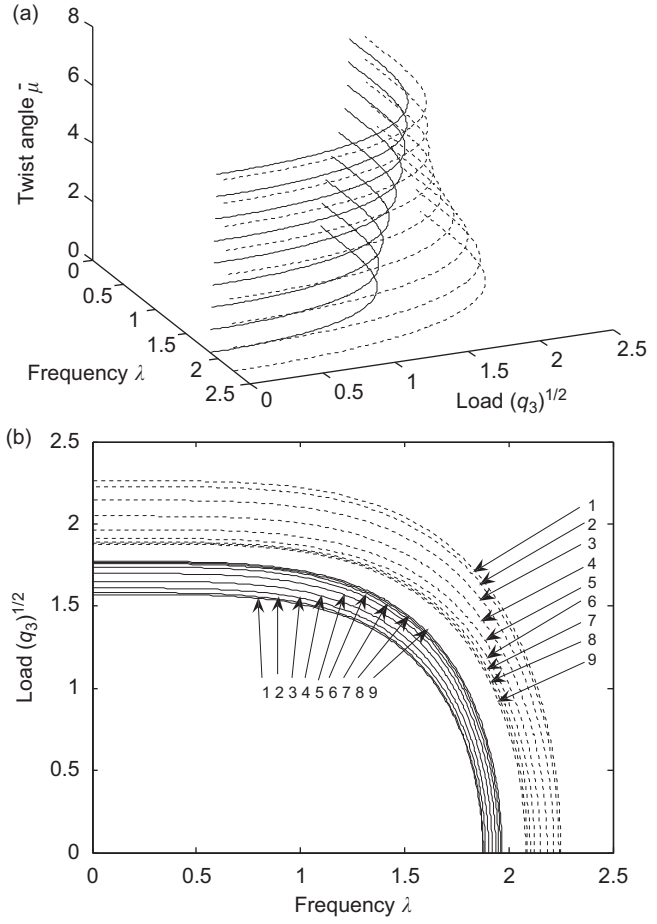

Fig. 5. The influence of the twist angle on interaction diagram of natural frequencies and buckling compressions: (a) 3D view, and (b) top view.

6. Numerical examples

6.1. Results comparison

6.1.1. Natural frequency convergence study and compared with existed solutions

Considering a cantilevered beam has a length of l=3.048 m with a pre-twist angle $\overline{\mu}=2\pi/9$ as the first example [14,19,20]. The properties of the beam are: $E=70\times10^9\,\mathrm{N/m^2}$, $G=27\times10^9\,\mathrm{N/m^2}$, $\rho=2700\,\mathrm{kg/m^3}$, $A=0.0127667\,\mathrm{m^2}$, $EI_x=2869.7\,\mathrm{N\cdot m^2}$, $EI_y=57393\,\mathrm{N\cdot m^2}$. The present frequencies ω(rad/s) are compared with Rosen [14], Banerjee [19,20] in Table 1. It is found that when taking shear effective factor as k=1/1.2, the polynomial terms p=12, the present results fit well with Banerjee's Timoshenko theory results. Therefore, the polynomial terms p=12 will be chosen for the study in this paper.

6.1.2. Comparison with results of ANSYS

Consider a clamped free beam with rectangular solid section as shown in Fig. 3 having the following properties:

Young's modulus E=200 Mpa, shear modulus $G=E/2(1+\nu)$, and shear effective factor k=1, Poisson's ratio ν=0.3 and the mass density ρ=7.8 kg/m^3, with length l=1 m, cross-section b=1/1.5 mm and d=1.5 mm, the area $A=bd$=1 mm^2, the second moment of area $I_1=1/12db^3$, $I_2=1/12bd^3$, and the polar moment of area $I_0=I_1+I_2=0.2245\,\mathrm{mm^4}$, when $b\le d$, the exact expressions of the torsion constant J has been given by Conner [38], having the value of 0.1067 mm^4.

To show the accuracy of the present method, the natural frequency λ and buckling loads $\sqrt{q_1}$, $\sqrt{q_2}$, $\sqrt{q_3}$ obtained by p-element are compared with the results of ANSYS [39] (choosing 100 BEAM188 elements in ANSYS) in Table 2, and good agreement is found. Since it is hard to apply pure bending moments or torque on beam element in ANSYS, the buckling moments (and torque) $\sqrt{m_1}$, $\sqrt{m_2}$, and m_3 obtained by p-element are not be able to compare with those of ANSYS. For a pre-twisted beam, the value of the buckling torque obtained in the same direction with the pre-twist angle is different

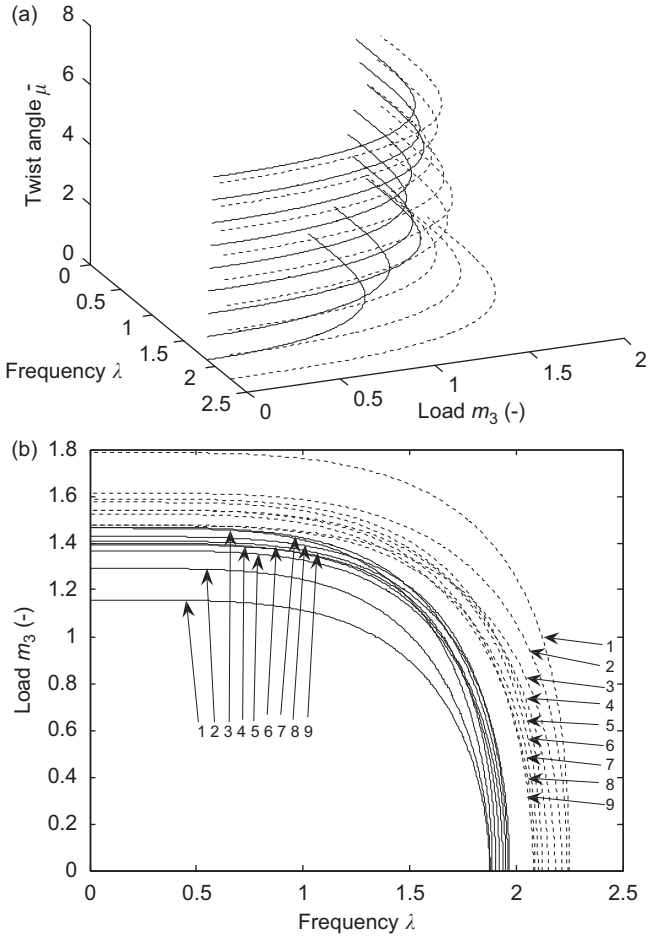

Fig. 6. The influence of the angle of twist on interaction diagram of natural frequencies and buckling torques m_3 (−): (a) 3D view, and (b) top view.

from that in the opposite direction (negative pre-twist). Then, the buckling torque in the same direction with the pre-twist angle is defined as m_3 (+) and the opposite one is m_3 (−). Conventionally, torsion constant J is taken equal to polar moment of area I_0 in beam vibration and buckling analysis. Actually, when the aspect ratio d/b becomes larger for rectangular cross-sections, the value of J has a great difference with I_0. Therefore, the relative error by taken ($J=I_0$) with ($J\neq I_0$) for frequency λ and buckling load parameters $\sqrt{q_1}$, $\sqrt{q_2}$, $\sqrt{q_3}$, $\sqrt{m_1}$, $\sqrt{m_2}$ and m_3 are computed in Table 3. As shown in Table 3, the results by taking ($J=I_0$) have a 21 percent difference with the accurate results by taking ($J\neq I_0$) for the first six modes of shear buckling loads $\sqrt{q_1}$, $\sqrt{q_2}$ and moments $\sqrt{m_1}$, $\sqrt{m_2}$, but the difference between J and I_0 has very little influence on the first six modes of axial loads $\sqrt{q_3}$ and buckling torques m_3. Therefore, in this paper we take ($J\neq I_0$) for more accurate solutions. In the presentation, we use λ instead of λ^2 to get an even spread between modes. Similarly, we use $\sqrt{q_i}$ and $\sqrt{m_i}$ instead of q_i and m_i.

6.2. The influence of rigidity ratio and pre-twisted angle

We are interested to find out the influence of the initial twist angle $\overline{\mu}$ on the static instability phenomena when the twisted beam is subjected to different external forces. The non-dimensional parameter $\overline{\mu}$ is taken varying from 0 to 2π. Let the area $A=bd$ to be constant equal to 1 mm^2 and the width d varied from 1 to 1.4 mm. And the shear effective factor is chosen as 1/1.2 in this section. The flexural rigidity ratios defined as $r=I_2/I_1$ varied with respect to the width d are given in Table 4. The influence of pre-twist angle $\overline{\mu}$ and flexural rigidity ratio r on the first two modes of natural vibration frequencies λ and buckling loads, including shear forces $\sqrt{q_1}$ and $\sqrt{q_2}$, axial force $\sqrt{q_3}$ bending moments $\sqrt{m_1}$, $\sqrt{m_2}$ and torque m_3 are tabulated in Table 5a–h, respectively. Meanwhile, the first two modes of frequency and buckling loads varying with the initial twist angle are shown graphically in Fig. 4(a–h), respectively. The solid lines and dotted lines as shown in Fig. 4 represent the first modes and second modes of the frequency or buckling loads, respectively. The lines which marked by 'upward pointing triangle △', 'right-pointing triangle ▷', 'left-pointing triangle ◁', 'square □' or 'circle ◦' corresponding to the frequency or buckling loads of beams with rigidity ratio r_i, $i=1,2,3,4,5$, respectively. As shown in Fig. 4(a–h), when there is no pre-twist angle, the results are compared well with existing literatures. The natural

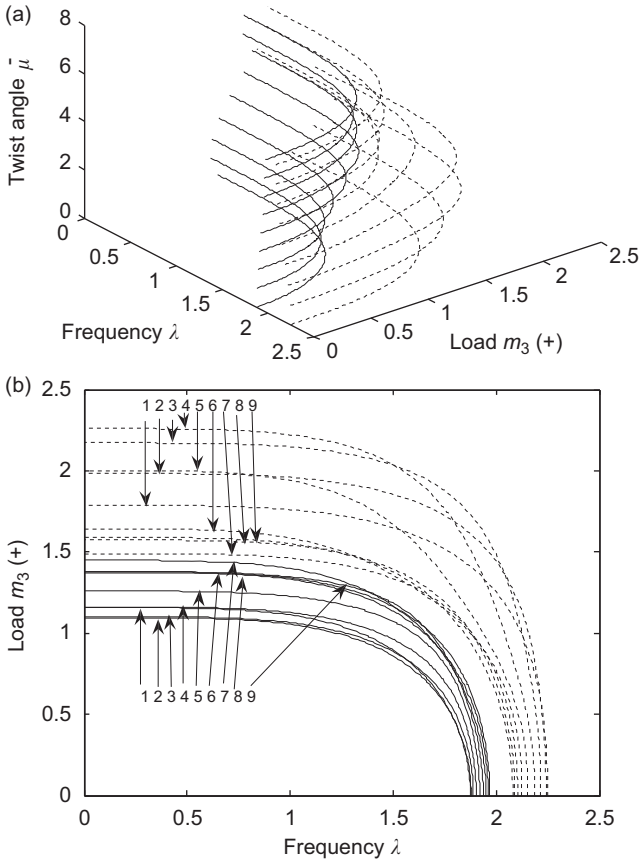

Fig. 7. The influence of the angle of twist on interaction diagram of natural frequencies and buckling torques m_3 (+): (a) 3D view, and (b) top view.

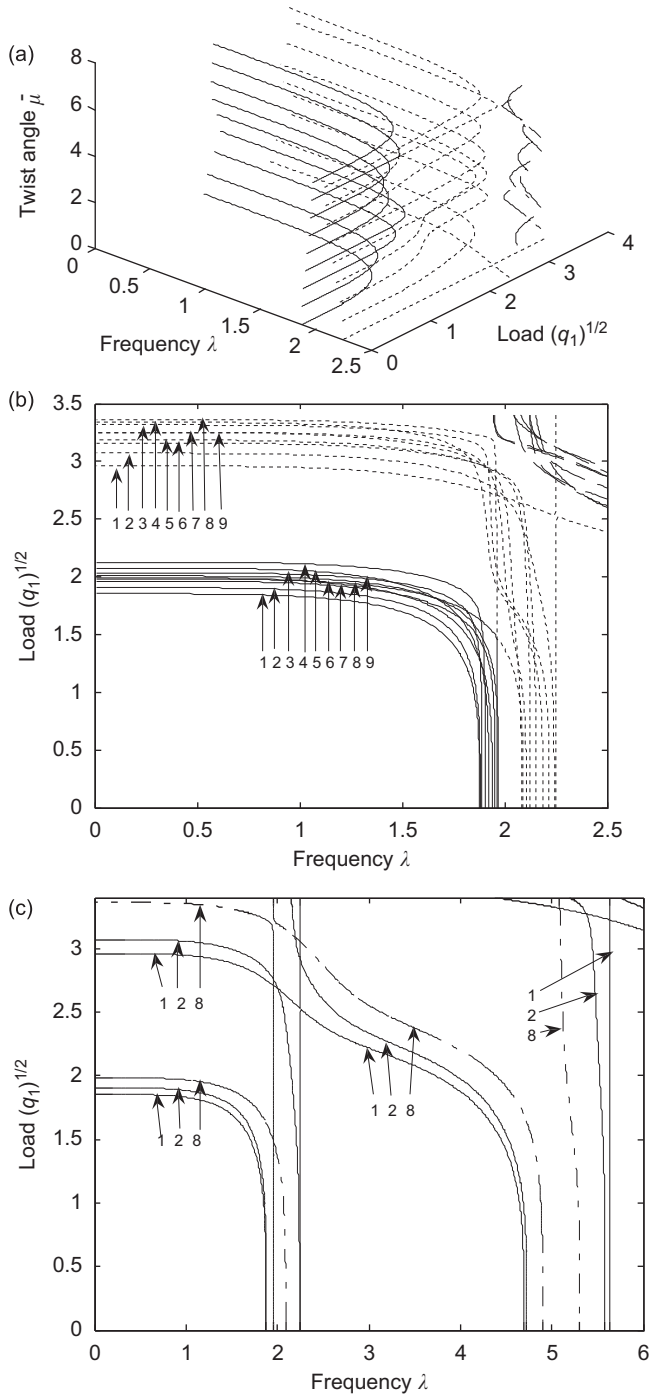

Fig. 8. The influence of the angle of twist on interaction diagram of natural frequency and shear buckling loads $\sqrt{q_1}$: (a) 3D view, (b) top view, and (c) top view for $\overline{\mu}_i$ $(i=1,2,8)$.

frequencies and/or buckling loads for rigidity ratio $r_1=1$ (i.e. square cross-sections beams) are kept constant with the twist angle. It is observed in Fig. 4a and b that the first modes of the frequency and axial loads are increasing with the pre-twist angle and the rigidity ratio while the second modes decreased. As shown in Fig. 4d for $\sqrt{q_2}$ and Fig. 4e for $\sqrt{m_1}$, both the first two buckling loads are increasing with the rigidity ratio monotonically. However, the buckling loads are not monotonically with respect to the pre-twist angle. Similar phenomenon can be found with $\sqrt{q_1}$ in Fig. 4c and $\sqrt{m_2}$ in Fig. 4f. The situations for the first two buckling modes of torque m_3 $(-)$ or m_3 $(+)$ become more complicated. It is observed

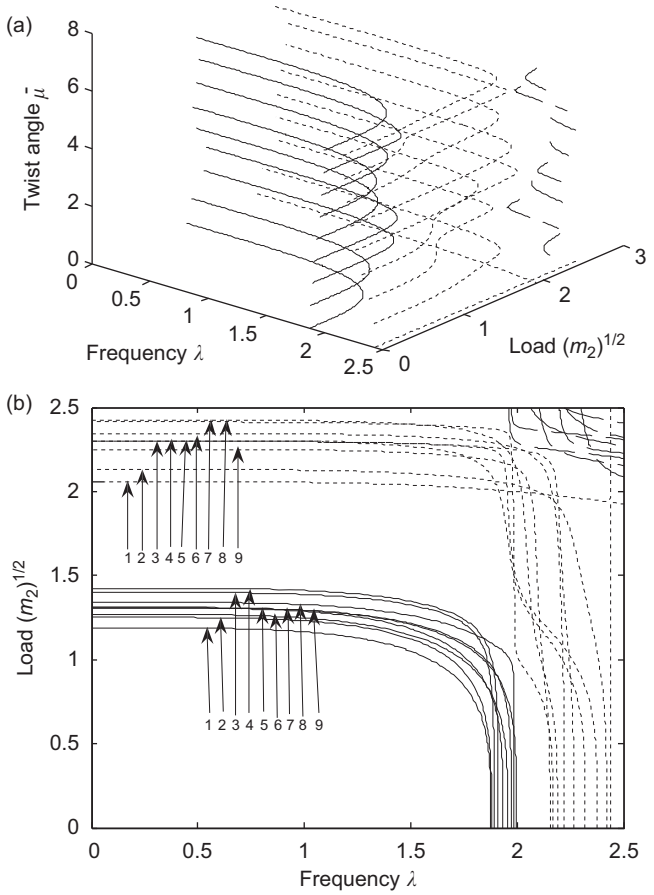

Fig. 9. The influence of the angle of twist on the interaction diagram of natural frequency and buckling moments $\sqrt{m_2}$: (a) 3D view, and (b) top view.

that the torques are not affected monotonically neither by the rigidity ratio nor with the twist angle as shown in Table 5g–h and Fig. 4g–h.

6.3. *Interaction of natural frequency and buckling loads*

Consider the dynamic buckling of a rectangular solid section column clamped at one end and free at the other end having the properties along the principal axes for Poisson's ratio 0.3 and effective shear area $k=1/1.2$ as in Section 6.2. The beam has a width $d=1.2$ mm and $b=1/1.2$ mm, with the rigidity ratio $r=1.2^4$. The interactions of natural frequency and buckling loads under the influence of the angle of pre-twist $\overline{\mu}_i=(i-1)\pi/4$, $i=1,2,\ldots,9$ are considered. In this section, the first, second and third modes of the interaction diagrams are distinguished by solid-lines, dotted-lines and dashed-lines respectively.

6.3.1. *Interaction of natural frequency and buckling compression*

The interaction of natural frequency and buckling compression under the influence of the angle of twist is computed in Figs. 5(a) and (b). Fig. 5(a) shows the variation of the dynamic buckling loads with the twist angle and Fig. 5(b) shows the top view. The numbers of the twist angle $\overline{\mu}_i=(i-1)\pi/4$, where i varied from 1 to 9 are marked in Fig. 5b. The first two natural frequencies for the un-twisted beam are 1.8751 and $1.8751\times r^{1/4}=2.2501$ and the first two buckling compressions are $\pi/2=1.5708$ and $1.5708\times r^{1/2}=2.2619$ as expected. It is interesting to note that the first mode increases together with the angle of twist but the second decreases seeming to close the first two modes together. The gaps close monotonically as the angle of twist increases for natural frequencies and buckling compressions.

6.3.2. *Interaction of natural frequency and buckling torques*

The interaction of natural frequency and buckling torque under the influence of the pre-twist angle is computed in Figs. 6(a) and (b). Fig. 6(a) shows the variation of the dynamic buckling torques with the twist angle and Fig. 6(b) shows the

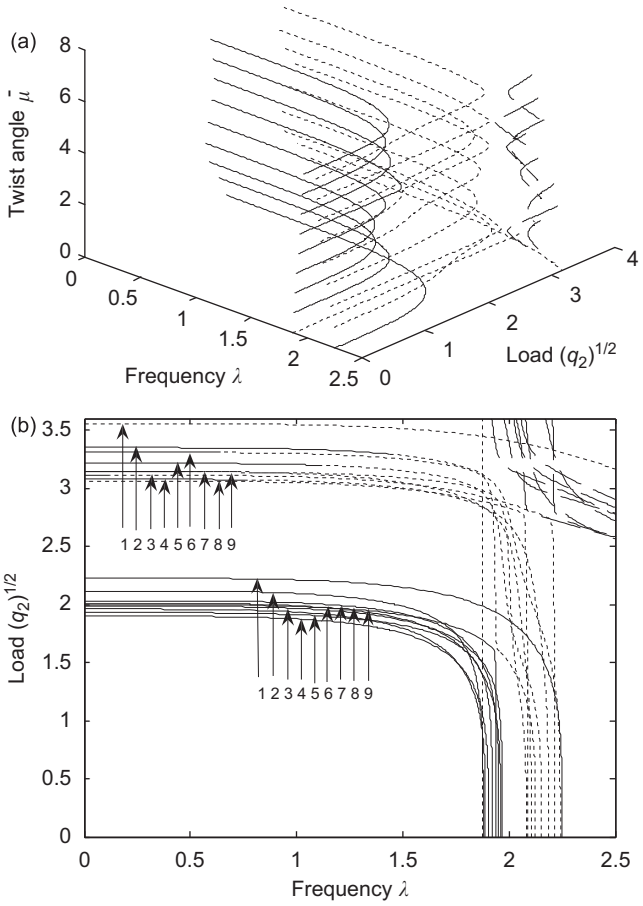

Fig. 10. The influence of the angle of twist on interaction diagram of natural frequency and shear buckling loads $\sqrt{q_2}$: (a) 3D view, and (b) top view.

top view where the twist angle is numbered. The first two natural frequencies for the un-twisted beam are 1.8751 and 2.2501 as in Section 6.3.1 and the first two buckling torques are 1.1570 and 1.7867 (comparing to 1.1570 and 1.7867 for Euler assumption [36]) as expected. It is noted that the two frequency modes increases together with the angle of twist. However, unlike natural frequencies and compressions, the closeness is not monotonic for buckling torque, where the gaps are smallest near the twist angle $\overline{\mu} = 3\pi/2$. Similar phenomenon can be found for the buckling torque $m3$ (+) shown in Figs. 7(a and b).

6.3.3. *Interaction of natural frequency and shear buckling loads $\sqrt{q_1}$ and moments $\sqrt{m_2}$*

Since the internal forces along the length of the pre-twist beam due to loads $\sqrt{q_1}$ or $\sqrt{m_2}$ are very similar, the interaction of natural frequency and shear buckling loads $\sqrt{q_1}$ or $\sqrt{m_2}$ under the influence of the pre-twist angle are considered together in this section, as shown in Figs. 8 and 9, respectively. The variation of the dynamic buckling loads with the twist angle and the top view are shown as the previous sections. When there is no pre-twist, the straight beam will only buckle about axis 1 under shear load $\sqrt{q_1}$ as shown in Fig. 8 or moment $\sqrt{m_2}$ as shown in Fig. 9. The first vibration mode begins at the point (frequency λ=1.8751, loads $\sqrt{q_1}$ or $\sqrt{m_2}$=0), and ends at the buckling mode (λ=0 and $\sqrt{q_1} = 1.8534$, or $\sqrt{m_2} = 1.1596$ (as expected in Timoshenko [40])). Since the beam will not buckle about axis 2, the second vibration mode beginning at the point (λ=2.2501, $\sqrt{q_1}$ or $\sqrt{m_2} = 0$) is a straight line vertical to the frequency axis. When a pre-twist angle exists, the case $\overline{\mu} = \pi/4$ (i=2) is taken as an example to compare with $\overline{\mu} = 0$, (i=1) as shown in Fig. 8(c). To show the first four frequency modes, the frequency axis is extended from (0, 2.5) given in Fig. 8(b) to (0, 6) as shown in Fig. 8(c). When $\overline{\mu} = \pi/4$ the beam will buckle about axis 1, beginning at the first frequency mode value λ=1.8786, and ending at the first buckling loads mode value $\sqrt{q_1} = 1.9064$. Meanwhile, the beam will also buckle about axis 2, corresponding to the second frequency mode value λ=2.2412 and the second buckling mode loads $\sqrt{q_1} = 3.0709$. While for a no pre-twist beam, it is the third frequency mode λ=4.6941 rather than the second mode (λ=2.2501) to buckle at the second buckling mode load $\sqrt{q_1} = 2.9617$. And as shown in Fig. 8(b), although the buckling capacity for the pre-twisted beams is not increased monotonically with the twist angle, the buckling capacity is enhanced when compared with a no

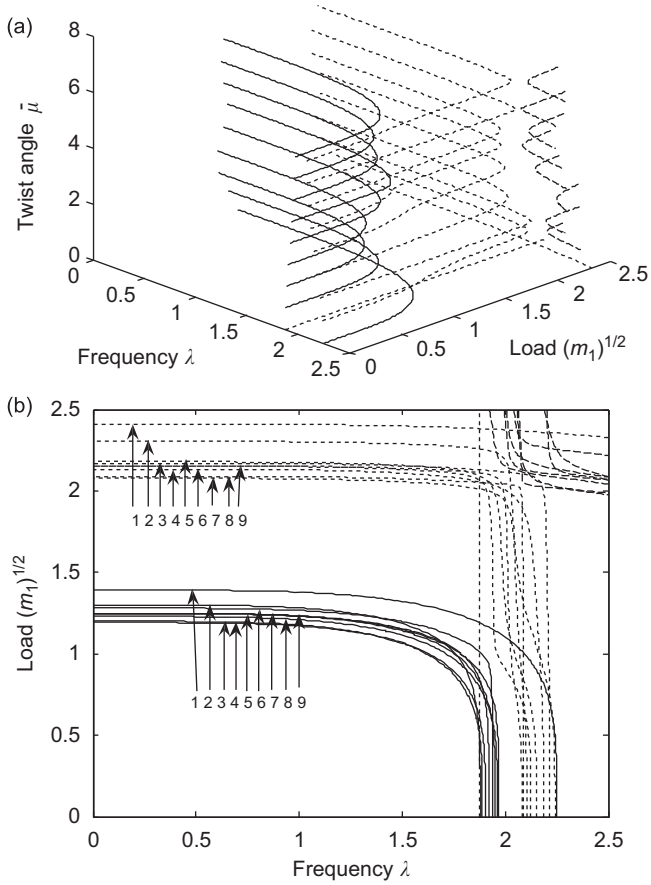

Fig. 11. The influence of the angle of twist on the interaction diagram of natural frequency and buckling moments $\sqrt{m_1}$: (a) 3D view, and (b) top view.

pre-twist beam. It is interesting to note that when $\bar{\mu}=7\pi/4$, (i=8) i.e., the lines numbered as the 8th lines in Fig. 8(b) for $\sqrt{q_1}$ or Fig. 9(b) for $\sqrt{m_2}$, the interaction diagrams beginning at the first frequency mode seems to end at the second buckling mode, and the lines starting at the second frequency mode will finally buckle at the first buckling mode, a more detail view can be seen from the lines numbered as the 8th lines given in Fig. 8(c).

6.3.4. Interaction of natural frequency and shear buckling loads $\sqrt{q_2}$ and moments $\sqrt{m_1}$

In this example, the interaction of natural frequency and shear buckling loads $\sqrt{q_2}$ or $\sqrt{m_1}$ under the influence of the angle of twist are computed in Figs. 10 and 11, respectively. When there is no pre-twist, the beam will only buckle about axis 2, starting at the frequency point 2.2501. While when once a pre-twist is presented, the first buckling mode of the interaction diagram will start at frequency point 1.8751. Unlike the cases for buckling loads $\sqrt{q_1}$ or $\sqrt{m_2}$, the buckling capacity of the beam under loads $\sqrt{q_2}$ or $\sqrt{m_1}$ are weakened by the pre-twist angle. When $\bar{\mu}=5\pi/4$ numbered as the 6th lines for interaction diagram of frequency with buckling load $\sqrt{q_2}$ or buckling moment $\sqrt{m_1}$ as shown in Figs. 10(b) and 11(b), an avoid crossing phenomenon appears which indicates that the interaction diagram beginning at the first frequency mode will finally buckle at the second buckling mode, and the interaction diagram starting at the second frequency mode will end at the first buckling mode.

7. Conclusions

The influence of multiple kinds of initial stresses due to compression, shears, moments and torque on the natural vibration of pre-twisted straight beam based on the Timoshenko theory has been formulated successfully with the use of three-dimensional Green strain tensor. The Frenet formulae in differential geometry were employed to treat the pre-twist. The governing equations and the associated natural boundary conditions were derived from the variational principle. It is noted that the first two modes tend to close together as the angle of twist increases. The gaps reduce monotonically as the

angle of twist increases. However, unlike natural frequencies and compression compressions, the closeness is not monotonic for buckling shears, moments and torques.

Acknowledgement

The research is fully supported by the Research Grant Council of Hong Kong grant number 116608.

Appendix A

C^0 hierarchical shape functions:

$$f_1=(1-\xi)/2$$

$$f_2=(1+\xi)/2$$

$$f_3=(\xi^2-1)/2$$

$$f_4=(\xi^3-\xi)/2$$

$$f_5=(5\xi^4-6\xi^2+1)/8$$

$$f_6=(7\xi^5-10\xi^3+3\xi)/8$$

$$f_7=(63\xi^6-105\xi^4+45\xi^2-3)/48$$

$$f_8=(99\xi^7-189\xi^5+105\xi^3-15\xi)/48$$

$$f_9=(429\xi^8-924\xi^6+630\xi^4-140\xi^2+5)/128$$

$$f_{10}=(715\xi^9-1716\xi^7+1386\xi^5-420\xi^3+35\xi)/128$$

$$f_{11}=(2431\xi^{10}-6435\xi^8+6006\xi^6-2310\xi^4+315\xi^2-7)/256$$

$$f_{12}=(4199\xi^{11}-12155\xi^9+12870\xi^7-6006\xi^5+1155\xi^3-63\xi)/256$$

$$f_{13}=(29393\xi^{12}-92378\xi^{10}+109395\xi^8-60060\xi^6+15015\xi^4-1386\xi^2+21)/1024$$

$$f_{14}=(52003\xi^{13}-176358\xi^{11}+230945\xi^9-145860\xi^7+45045\xi^5-6006\xi^3+231\xi)/1024$$

where $-1<\xi<1$. By mapping ξ from $(-1,\ 1)$ to $(0,\ 1)$, the hierarchical shape functions $f_i(\xi)$ mapped into $\overline{f}_i(\xi)\ (0<\xi<1)$are used in this paper.

Appendix B

The non-zero coefficients of the stiffness matrix $\overline{\mathbf{K}}^e$ are:

m	n	$\overline{\mathbf{K}}^e_{m,n}$
$6i-5$	$6j-5$	$A^{0,0}_{i,j}\cdot\overline{\mu}^2\cdot g+A^{1,1}_{i,j}\cdot g$
$6i-4$	$6j-5$	$-A^{1,0}_{i,j}\cdot\overline{\mu}\cdot g+A^{0,1}_{i,j}\cdot\overline{\mu}\cdot g$
$6i-2$	$6j-5$	$-A^{0,0}_{i,j}\cdot\overline{\mu}\cdot g$
$6i-1$	$6j-5$	$-A^{0,1}_{i,j}\cdot g$
$6i-5$	$6j-4$	$A^{1,0}_{i,j}\cdot\overline{\mu}\cdot g-A^{0,1}_{i,j}\cdot\overline{\mu}\cdot g$
$6i-4$	$6j-4$	$A^{0,0}_{i,j}\cdot\overline{\mu}^2\cdot g+A^{1,1}_{i,j}\cdot g$
$6i-2$	$6j-4$	$A^{0,1}_{i,j}\cdot g$
$6i-1$	$6j-4$	$-A^{0,0}_{i,j}\cdot\overline{\mu}\cdot g$
$6i-3$	$6j-3$	$A^{1,1}_{i,j}/r_1$
$6i-5$	$6j-2$	$-A^{0,0}_{i,j}\cdot\overline{\mu}\cdot g$
$6i-4$	$6j-2$	$A^{1,0}_{i,j}\cdot g$
$6i-1$	$6j-2$	$A^{0,0}_{i,j}\cdot(g\cdot r_1+r_2\cdot\overline{\mu}^2)/r_1+A^{1,1}_{i,j}$

$6i-1$	$6j-2$	$-A_{i,j}^{1,0}\cdot\overline{\mu}\cdot r_2/r_1+A_{i,j}^{0,1}\cdot\overline{\mu}$
$6i-5$	$6j-1$	$-A_{i,j}^{1,0}\cdot g$
$6i-4$	$6j-1$	$-A_{i,j}^{0,0}\cdot\overline{\mu}\cdot g$
$6i-2$	$6j-1$	$A_{i,j}^{1,0}\cdot\overline{\mu}-A_{i,j}^{0,1}\cdot\overline{\mu}\cdot r_2/r_1$
$6i-1$	$6j-1$	$A_{i,j}^{0,0}\cdot(g+\overline{\mu}^2)+A_{i,j}^{1,1}\cdot r_2/r_1$
$6i$	$6j$	$A_{i,j}^{1,1}\cdot g\cdot r_J$

The non-zero coefficients of the mass matrix $\overline{\mathbf{M}}^e$ are:

m	n	$\overline{\mathbf{M}}_{m,n}^e$
$6i-5$	$6j-5$	$A_{i,j}^{0,0}$
$6i-4$	$6j-4$	$A_{i,j}^{0,0}$
$6i-3$	$6j-3$	$A_{i,j}^{0,0}$
$6i-2$	$6j-2$	$A_{i,j}^{0,0}\cdot r_1$
$6i-1$	$6j-1$	$A_{i,j}^{0,0}\cdot r_2$
$6i$	$6j$	$A_{i,j}^{0,0}\cdot r_0$

The non-zero coefficients of the geometric stiffness matrix $\overline{\mathbf{G}}_{q_3}^e$ are:

m	n	$\overline{\mathbf{G}}_{m,n}^e$
$6i-5$	$6j-5$	$A_{i,j}^{0,0}\cdot\overline{\mu}^2+A_{i,j}^{1,1}$
$6i-4$	$6j-5$	$-A_{i,j}^{1,0}\cdot\overline{\mu}+A_{i,j}^{0,1}\cdot\overline{\mu}$
$6i-5$	$6j-4$	$A_{i,j}^{1,0}\cdot\overline{\mu}-A_{i,j}^{0,1}\cdot\overline{\mu}$
$6i-4$	$6j-4$	$A_{i,j}^{0,0}\cdot\overline{\mu}^2+A_{i,j}^{1,1}$
$6i-3$	$6j-3$	$A_{i,j}^{1,1}$
$6i-2$	$6j-2$	$A_{i,j}^{0,0}\cdot r_2\cdot\overline{\mu}^2+A_{i,j}^{1,1}\cdot r_1$
$6i-1$	$6j-2$	$-A_{i,j}^{1,0}\cdot\overline{\mu}\cdot r_2+A_{i,j}^{0,1}\cdot\overline{\mu}\cdot r_1$
$6i-2$	$6j-1$	$A_{i,j}^{1,0}\cdot\overline{\mu}\cdot r_1-A_{i,j}^{0,1}\cdot\overline{\mu}\cdot r_2$
$6i-1$	$6j-1$	$A_{i,j}^{0,0}\cdot r_1\cdot\overline{\mu}^2+A_{i,j}^{1,1}\cdot r_2$
$6i$	$6j$	$A_{i,j}^{1,1}\cdot r_J$

The non-zero coefficients of the geometric stiffness matrix $\overline{\mathbf{G}}_{m_3}^e$ are:

m	n	$\overline{\mathbf{G}}_{m,n}^e$
$6i-2$	$6j-2$	$2A_{i,j}^{0,0}\cdot\overline{\mu}\cdot r_2/r_1$
$6i-1$	$6j-2$	$-A_{i,j}^{1,0}\cdot r_2/r_1+A_{i,j}^{0,1}$
$6i-2$	$6j-1$	$A_{i,j}^{1,0}-A_{i,j}^{0,1}\cdot r_2/r_1$
$6i-1$	$6j-1$	$2A_{i,j}^{0,0}\cdot\overline{\mu}$

The non-zero coefficients of the geometric stiffness matrix $\overline{\mathbf{G}}_{q_1}^e$ are:

m	n	$\overline{\mathbf{G}}_{m,n}^e$
$6i$	$6j-5$	$-B_{i,j}^{0,0}\cdot\overline{\mu}+C_{i,j}^{1,0}\cdot\overline{\mu}+D_{i,j}^{0,1}-E_{i,j}^{1,1}$
$6i$	$6j-4$	$D_{i,j}^{0,0}\cdot\overline{\mu}-E_{i,j}^{1,0}\cdot\overline{\mu}+B_{i,j}^{0,1}-C_{i,j}^{1,1}$
$6i-2$	$6j-3$	$-D_{i,j}^{0,1}-C_{i,j}^{0,1}\cdot\overline{\mu}+E_{i,j}^{1,1}$
$6i-1$	$6j-3$	$E_{i,j}^{0,1}\cdot\overline{\mu}-B_{i,j}^{0,1}+C_{i,j}^{1,1}$
$6i-3$	$6j-2$	$-D_{i,j}^{1,0}-C_{i,j}^{1,0}\cdot\overline{\mu}+E_{i,j}^{1,1}$
$6i-3$	$6j-1$	$E_{i,j}^{1,0}\cdot\overline{\mu}-B_{i,j}^{1,0}+C_{i,j}^{1,1}$
$6i-5$	$6j$	$-B_{i,j}^{0,0}\cdot\overline{\mu}+D_{i,j}^{1,0}+C_{i,j}^{0,1}\cdot\overline{\mu}-E_{i,j}^{1,1}$
$6i-4$	$6j$	$D_{i,j}^{0,0}\cdot\overline{\mu}+B_{i,j}^{1,0}-E_{i,j}^{0,1}\cdot\overline{\mu}-C_{i,j}^{1,1}$

The non-zero coefficients of the geometric stiffness matrix $\overline{\mathbf{G}}^e_{q_2}$ are:

m	n	$\overline{\mathbf{G}}^e_{m,n}$
$6i$	$6j-5$	$-D^{0,0}_{i,j}\cdot\overline{\mu}+E^{1,0}_{i,j}\cdot\overline{\mu}-B^{0,1}_{i,j}+C^{1,1}_{i,j}$
$6i$	$6j-4$	$-B^{0,0}_{i,j}\cdot\overline{\mu}+C^{1,0}_{i,j}\cdot\overline{\mu}+D^{0,1}_{i,j}-E^{1,1}_{i,j}$
$6i-2$	$6j-3$	$B^{0,1}_{i,j}-E^{0,1}_{i,j}\cdot\overline{\mu}-C^{1,1}_{i,j}$
$6i-1$	$6j-3$	$-C^{0,1}_{i,j}\cdot\overline{\mu}-D^{0,1}_{i,j}+E^{1,1}_{i,j}$
$6i-3$	$6j-2$	$B^{1,0}_{i,j}-E^{1,0}_{i,j}\cdot\overline{\mu}-C^{1,1}_{i,j}$
$6i-3$	$6j-1$	$-C^{1,0}_{i,j}\cdot\overline{\mu}-D^{1,0}_{i,j}+E^{1,1}_{i,j}$
$6i-5$	$6j$	$-D^{0,0}_{i,j}\cdot\overline{\mu}-B^{1,0}_{i,j}+E^{0,1}_{i,j}\cdot\overline{\mu}+C^{1,1}_{i,j}$
$6i-4$	$6j$	$-B^{0,0}_{i,j}\cdot\overline{\mu}+D^{1,0}_{i,j}+C^{0,1}_{i,j}\cdot\overline{\mu}-E^{1,1}_{i,j}$

The non-zero coefficients of the geometric stiffness matrix $\overline{\mathbf{G}}^e_{m_1}$ are:

m	n	$\overline{\mathbf{G}}^e_{m,n}$
$6i$	$6j-5$	$-D^{1,0}_{i,j}\cdot\overline{\mu}-B^{1,1}_{i,j}$
$6i$	$6j-4$	$-B^{1,0}_{i,j}\cdot\overline{\mu}+D^{1,1}_{i,j}$
$6i-2$	$6j-3$	$D^{0,1}_{i,j}\cdot\overline{\mu}+B^{1,1}_{i,j}$
$6i-1$	$6j-3$	$B^{0,1}_{i,j}\cdot\overline{\mu}-D^{1,1}_{i,j}$
$6i-3$	$6j-2$	$D^{1,0}_{i,j}\cdot\overline{\mu}+B^{1,1}_{i,j}$
$6i-3$	$6j-1$	$B^{1,0}_{i,j}\cdot\overline{\mu}-D^{1,1}_{i,j}$
$6i-5$	$6j$	$-D^{0,1}_{i,j}\cdot\overline{\mu}-B^{1,1}_{i,j}$
$6i-4$	$6j$	$-B^{0,1}_{i,j}\cdot\overline{\mu}+D^{1,1}_{i,j}$

The non-zero coefficients of the geometric stiffness matrix $\overline{\mathbf{G}}^e_{m_2}$ are:

m	n	$\overline{\mathbf{G}}^e_{m,n}$
$6i$	$6j-5$	$B^{1,0}_{i,j}\cdot\overline{\mu}-D^{1,1}_{i,j}$
$6i$	$6j-4$	$-D^{1,0}_{i,j}\cdot\overline{\mu}-B^{1,1}_{i,j}$
$6i-2$	$6j-3$	$-B^{0,1}_{i,j}\cdot\overline{\mu}+D^{1,1}_{i,j}$
$6i-1$	$6j-3$	$D^{0,1}_{i,j}\cdot\overline{\mu}+B^{1,1}_{i,j}$
$6i-3$	$6j-2$	$-B^{1,0}_{i,j}\cdot\overline{\mu}+D^{1,1}_{i,j}$
$6i-3$	$6j-1$	$D^{1,0}_{i,j}\cdot\overline{\mu}+B^{1,1}_{i,j}$
$6i-5$	$6j$	$B^{0,1}_{i,j}\cdot\overline{\mu}-D^{1,1}_{i,j}$
$6i-4$	$6j$	$-D^{0,1}_{i,j}\cdot\overline{\mu}-B^{1,1}_{i,j}$

The integrals are

$$A^{\alpha,\beta}_{i,j}=\int_0^1 \overline{f}^{\alpha}_i\cdot\overline{f}^{\beta}_j\,\mathrm{d}\xi$$

$$B^{\alpha,\beta}_{i,j}=\int_0^1 \cos[\overline{\mu}\cdot(1-\xi)]\cdot\overline{f}^{\alpha}_i\cdot\overline{f}^{\beta}_j\,\mathrm{d}\xi$$

$$C^{\alpha,\beta}_{i,j}=\int_0^1 \cos[\overline{\mu}\cdot(1-\xi)]\cdot(1-\xi)\cdot\overline{f}^{\alpha}_i\cdot\overline{f}^{\beta}_j\,\mathrm{d}\xi$$

$$D^{\alpha,\beta}_{i,j}=\int_0^1 \sin[\overline{\mu}\cdot(1-\xi)]\cdot\overline{f}^{\alpha}_i\cdot\overline{f}^{\beta}_j\,\mathrm{d}\xi$$

$$E^{\alpha,\beta}_{i,j}=\int_0^1 \sin[\overline{\mu}\cdot(1-\xi)]\cdot(1-\xi)\cdot\overline{f}^{\alpha}_i\cdot\overline{f}^{\beta}_j\,\mathrm{d}\xi$$

where $i=1,2,\ldots,p+2$, $j=1,2,\ldots,p+2$, and the superscript α and β ($\alpha,\beta=0,1$) denote the order of the derivatives with respect to ξ, and $\overline{\mu},r_1,r_2,r_0,r_J,g$ are the non-dimensional parameters given in Eq. (29).

References

[1] D.D. Rosard, Natural frequencies of twisted cantilever beams, *Journal of Applied Mechanics* 20 (1953) 241–244.
[2] A. Troesch, M. Anliker, H. Ziegler, Lateral vibrations of twisted rods, *Quarterly of Applied Mathematics* 12 (1954) 163–173.
[3] R.C. Diprima, G.H. Handelman, Vibrations of twisted beams, *Quarterly of Applied Mathematics* 12 (1954) 241–259.
[4] W. Carnegie, Vibration of pre-twisted cantilever blading, *Proceedings of the Institution of Mechanical Engineers, London* 173 (1959) 343–346.
[5] W. Carnegie, J. Thomas, The coupled bending–bending vibration of pre-twisted tapered blading, *Journal of Engineering for Industry, American Society of Mechanical Engineers* 94 (1972) 255–266.
[6] H.A. Slyper, Coupled bending vibrations of pre-twisted cantilever beams, *Journal of Mechanical Engineering Science* 4 (1962) 365–379.
[7] M. Anliker, B.A. Troesch, Lateral vibrations of pre-twisted rods with various boundary conditions, *Zeitschrift fuer Angewandte Mathematik und Physik* 14 (1963) 218–236.
[8] B. Dawson, Coupled bending vibrations of pre-twisted cantilever blading treated by Rayleigh–Ritz method, *Journal of Mechanical Engineering Science* 10 (1968) 381–386.
[9] S.M. Lin, Vibrations of elastically restrained non-uniform beams with arbitrary pre-twist, *American Institute of Aeronautics and Astronautics Journal* 35 (1977) 1681–1687.
[10] R.S. Gupta, J.S. Rao, Finite element eigenvalue analysis of tapered and twisted Timoshenko beams, *Journal of Sound and Vibration* 56 (1978) 187–200.
[11] F. Sisto, A.T. Chang, A finite element for vibration analysis of twisted blades based on beam theory, *American Institute of Aeronautics and Astronautics Journal* 22 (1984) 1646–1651.
[12] B. Yardimoglu, T. Yildirim, Finite element model for vibration analysis of pre-twisted Timoshenko beam, *Journal of Sound and Vibration* 273 (2004) 741–754.
[13] Z. Celep, D. Turham, On the influence of pre-twisting on the vibration of beams including the shear and rotary inertia effects, *Journal of Sound and Vibration* 110 (1986) 523–528.
[14] A. Rosen, R.G. Loewy, B. Mathew, Use of twisted principal coordinates and non-physical coordinates in blade analysis, *Vertica* 11 (1987) 541–572.
[15] A. Rosen, Structural and dynamic behaviour of pre-twisted rods and beams, *Applied Mechanics Reviews* 44 (1991) 483–515.
[16] O. Onipede, S.B. Dong, J.B. Kosmatka, Natural vibrations and waves in pre-twisted rods, *Composites Engineering* 4–5 (1994) 487–502.
[17] A.S. Balhaddad, D. Onipede Jr., Three-dimensional free vibration of pre-twisted beams, *American Institute of Aeronautics and Astronautics Journal* 36 (1998) 1524–1528.
[18] E. Petrov, M. Geradin, Finite element theory for curved and twisted beams based on exact solutions for three dimensional solids. Part 1: beam concept and geometrically exact nonlinear formulation, part 2: anisotropic and advanced beam models, *Computer Methods in Applied Mechanics and Engineering* 165 (1998) 43–127.
[19] J.R. Banerjee, Free vibration analysis of a twisted beam using the dynamic stiffness method, *International Journal of Solids and Structures* 38 (2001) 6703–6722.
[20] J.R. Banerjee, Development of an exact dynamic stiffness matrix for free vibration analysis of a twisted Timoshenko beam, *Journal of Sound and Vibration* 270 (2004) 379–401.
[21] W.R. Chen, L.M. Keer, Transverse vibration of a rotating twisted Timoshenko beam under axial loadings, *ASME Journal of Vibrations and Acoustics* 115 (1993) 285–294.
[22] H.P. Lee, Buckling and dynamic stability of spinning pre-twisted beams under compressive axial loads, *International Journal of Mechanical Science* 36 (11) (1994) 1011–1026.
[23] C.L. Liao, B.W. Huang, Parametric instability of a spinning pre-twisted beam under periodic axial force, *International Journal of Mechanical Science* 37 (1995) 423–439.
[24] G. Sakar, M. Sabuncu, Buckling and dynamic stability of a rotating pre-twisted asymmetric cross-section blade subject to an axial periodic load, *Finite Elements in Analysis and Design* 40 (2001) 1399–1415.
[25] K.C. Liu, J. Friend, L. Yeo, The axial-torsional vibration of pre-twisted beams, *Journal of Sound and Vibration* 321 (1–2) (2009) 115–136.
[26] E.J. Sapountzakis, J.A. Dourakopoulos, Shear deformation effect in flexural-torsional vibrations of beams by BEM, *Acta Mechanica* 203 (3–4) (2009) 197–221.
[27] S.P. Machado, Non-linear buckling and postbuckling behavior of thin-walled beams considering shear deformation, *International Journal of Non-linear Mechanics* 43 (5) (2008) 345–365.
[28] S.K. Sinha, Combined torsional-bending axial dynamics of a twisted rotating cantilever Timoshenko beam with contact-impact loads at the free end, *Journal of Applied Mechanics-Transactions of the ASME* 74 (3) (2007) 505–522.
[29] J. Fan, X.C. Zhang, A.Y.T. Leung, D.W.S. Tsui, J.N. Xu, Fourier *p*-elements for dynamic stability of columns, *International Journal of Structural Stability and Dynamics* 7 (2007) 359–376.
[30] A.Y.T. Leung, B. Zhu, Fourier *p*-elements for curved beam vibrations, *Thin-walled structures* 42 (1) (2004) 39–57.
[31] N.S. Bardell, Free vibration analysis of a flat plate using the hierarchical finite element method, *Journal of Sound and Vibration* 151 (1992) 263–289.
[32] N.S. Bardell, The free vibration of skew plates using the hierarchical finite element method, *Computers and Structures* 45 (1992) 841–874.
[33] A. Houmat, Hierarchical finite element analysis of the vibration of membranes, *Journal of Sound and Vibration* 201 (4) (1997) 465–472.
[34] B. Zhu, p-version finite elements and applications in structural impact and damage detection, Ph.D. Thesis, 2005.
[35] A.Y.T. Leung, A comment on the article "Stability of tapered I-beams under torsional moments" by J.D. Yau,, *Finite Elements in Analysis and Design* 42 (2006) 914–927 (44 (2007) 86–87).
[36] A.Y.T. Leung, Exact dynamic stiffness for axial-torsional buckling of structural frames, *Thin-Walled Structures* 46 (2008) 1–10.
[37] A.Y.T. Leung, Letter to the Editor: a comment on the article "Rigid body concept for geometric nonlinear analysis of 3D frames, plates and shells based on the updated Lagrangian formulation" by Y.B. Yang, S.P. Lin, C.S. Chen, *Computer Methods in Applied Mechanics Engineering* 196 (2007) 1178–1192 (197 (2008) 879–880).
[38] J.J. Connor, *Analysis of Structural Member systems*, Ronald Press, New York, 1976 (p. 282).
[39] ANSYS Inc., 201 Johnson Road, Houston, PA 15342-1300, U.S.A.
[40] S.P. Timoshenko, J.M. Gere, *Theory of Elastic Stability*, McGraw-Hill, New York, 1961.